

DRL No. 216
DRD No. SE-2

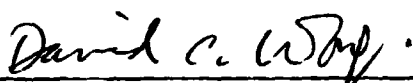
DOE/JPL 956831-1
Distribution Category UC-63

**PULSED EXCIMER LASER PROCESSING
FOR COST-EFFECTIVE SOLAR CELLS**

Quarterly Report No. 1

May - July 1984

Prepared By



D. Wong
Principal Investigator

Approved By



W. R. Bottenberg
Program Manager

**ARCO Solar, Inc.
P. O. Box 2105
Chatsworth, California 91311**

The JPL Flat-Plate Solar Array Project is sponsored by the U.S. Department of Energy and forms part of the solar Photovoltaic Conversion Program to initiate a major effort toward the development of low-cost solar arrays. This work was performed for the Jet Propulsion Laboratory, California Institute of Technology, by agreement between NASA and DOE.

This work was performed for the Jet Propulsion Laboratory, California Institute of Technology, and was sponsored by the U.S. Department of Energy through an agreement with the National Aeronautics and Space Administration.

This report was prepared as an account of work sponsored by an agency of the United States Government. Neither the United States Government nor any agency thereof, nor any of their employees, makes any warranty, express or implied, or assumes any legal liability or responsibility for the accuracy, completeness or usefulness of any information, apparatus, product or process disclosed, or represents that its use would not infringe privately owned rights.

Reference herein to any specific commercial product, process, or service by trade name, trademark manufacturer, or otherwise, does not necessarily constitute or imply its endorsement, recommendation, or favoring by the United States Government or any agency thereof. The views and opinions of authors expressed herein do not necessarily state or reflect those of the United States Government or any agency thereof.

ABSTRACT

The objective of this contract is to develop a solar cell process sequence that incorporates three process steps which use pulsed excimer lasers, to verify that this sequence yields high efficiency cells at a low cost, and to document the feasibility of carrying this technology from the laboratory bench scale to factory size. The three process steps are: junction formation, surface passivation, and front metallization. The effort is to take place during a one-year period.

During this reporting period, a series of annealing experiments were conducted. Parameter variations included beam energy density, percentage of beam overlap, sources of diffusant, and different surface conditions such as chemical-mechanical polished, caustic etched, and textured. Diffusant deposition included spin-on liquid dopant and ion implant.

Due to the lower surface reflectivity and the "wetting" effect by the spin-on source, textured wafers experienced more surface damage and stress than polished wafers. Maximum cell efficiency obtained for Cz polished wafers was 9% and for Cz textured wafers was 11.5% (no A/R). Surface damage limited the cell efficiency.

Laser annealing on ion-implanted wafers was conducted with phosphorus implant with acceleration energy of 10 keV at fluences of $1-5 \times 10^{15}$ atom/cm². Maximum cell efficiency was less than 8% (no A/R coating). Low J_{sc} , V_{oc} , and fill factor suggested incomplete implant damage removal.

Decreasing the implant voltage from 10 keV to 5 keV and increasing laser energy to above 0.9 J/cm², some cell efficiencies over 9.4% before A/R. The goal of producing cells of 16.5% has not materialized due to problems in ion implant uniformity, unavailable low keV ion implant, and laser beam inhomogeneity.

During the next period, work will focus on developing a 1 keV glow discharge capability and on fabrication of Boron implanted junctions on n type wafers.

CONTENTS

1.0	Introduction and Summary.....	1
2.0	Progress.....	3
2.1	Development of Process Sequence Selection.....	3
2.2	Laser Equipment.....	4
2.2.1	Small Scale Laser.....	4
2.2.1.1	Optical System.....	4
2.2.1.2	Computer Control System.....	9
2.2.1.3	Optical Diagnostics.....	9
2.2.2	High Energy Excimer Laser (Lucy).....	9
2.2.2.1	Motion Control and Laser Firing.....	11
2.2.2.2	Optical Diagnostics.....	13
2.2.3	Reticon Array for Beam Profiling.....	13
2.3	Quarterly Activities.....	23
3.0	Significant Experimental Results.....	29
3.1	Liquid Dopant.....	29
3.1.1	Textured Surface.....	29
3.1.2	Chemically Polished Surface.....	31
3.2	Ion Implanted Emitter.....	34
4.0	Discussion of Experimental Results.....	45
5.0	Target Process Selection Report.....	49
5.1	Process Selection.....	49
5.1.1	Baseline Prices.....	49
5.1.2	Description of the preliminary laser process..	51
5.2	Economic Analysis.....	53
5.2.1	Approach.....	53
5.2.2	Results.....	54
5.2.2.1	Discussion of Cost Elements of Excimer Laser Applications.....	58
5.2.3	IPEG Analysis of Specific Laser Processes.....	58
6.0	Program Status and Plans.....	63
	References.....	67

CONTENTS (continued)

Tables

1. Excimer laser annealing parameters.....	25
2. Textured Cz p-type wafer with spin-on source laser annealed:	
a. at 0.4 J/cm ² with 70% overlap.....	29
b. at 0.4 J/cm ² with 70% overlap followed by furnace heat treatment at 650°C for 30 minutes.....	31
c. at 0.7 J/cm ² with 50% overlap.....	31
3. Cells fabricated from polished Cz p-type wafer with spin-on source, laser annealed at energies: 0.9, 1.2 and 1.6 J/cm ²	32
4. Cell performance of thermally diffused wafers, caustic polished with spin-on source as dopant.....	34
5. Results of laser annealing for caustic polish, 10 keV ion implant with dosage 5x10 ¹⁵ and 1x10 ¹⁵ atoms/cm ² , respectively.....	34
6. Results of laser annealing for chem-mech polished wafers 5 keV ion implanted with 2.5x10 ¹⁵ atom/cm ² dosage.....	37
7. First experimental result with the large laser, "Lucy", at density 1.4 and 1.6 J/cm ² , respectively.....	39
8. Results of annealing by large laser with lower energy density and overlap %.....	41
9. Laser annealing for wafer with thermal N ⁺ deposition. Control cells were thermally diffused. All cells without A/R.....	42
10. Cost Summary - JPL Sample Sequence.....	55
11. Cost Summary - Proposed Laser Process.....	56

Figures

1. Laser annealing processes sequences for the First Quarter.....	3
2. Second phase process sequence.....	4
3. Laboratory arrangement for excimer laser processing of silicon solar cells.....	6
4. Excimer laser annealing facility.....	7
5. Typical laser pulse shapes used in laser annealing process studies.....	8

CONTENTS (continued)

6.	Scan patterns.....	10
7.	Laboratory layout for large excimer annealing process....	12
8.	Intensity vs. time from large x-ray preionized excimer laser using XeCl (308 nm).....	14
9.	Input He-Ne beam used for testing kaleidoscope beam homogenizer.....	16
10.	Optical set-up for kaleidoscope testing.....	17
11.	Beam profile at exit plane of kaleidoscope using f/4 optics.....	19
12.	Beam profile demagnified 2x and reimaged.....	20
13.	Beam profile at exit plane of kaleidoscope using f/6 input optics.....	21
14.	Profile of excimer output beam.....	22
15.	Quartery Activities.....	23
16.	500x SEM of textured surface (with spin-on liquid dopant) after laser annealing at (a) 0.4 J/cm^2 (b) 0.7 J/cm^2 and (c) 1.2 J/cm^2	30 31
17a.	Laser annealing (B7-3F) at 0.9 J/cm^2 on caustic polished surface with spin-on liquid dopant source. Heavy melting and surface damage are clearly shown.....	33
17b.	Pimple type crater defects on surface annealed at 1.2 J/cm^2	33
18a.	Electrical characteristics of a thermally diffused N+ spin-on liquid source on p substrates, light I-V.....	35
18b.	Electrical characteristics of a thermally diffused N+ spin-on liquid source on p substrates, dark I-V.....	36
19.	Baseline material characterization of FZ wafers by thermal (POCl_3) diffusion. Spin-on A/R coating.....	38
20.	Laser annealing on 5 KeV, $2.5 \times 10^{15} \text{ atom/cm}^2$ ion implanted surfaces at 1.3 J/cm^2 , with 70% overlap pulse duration estimated 6ns (B-9).....	40

CONTENTS (continued)

21a.	Light and dark I-V curves for typical cells from thermal N ⁺ deposition and diffusion.....	43
21b.	Light and dark I-V curves for typical cells from thermal N ⁺ deposition and laser drive at 1.25 J/cm ² , 10% overlap.....	44
22.	SIMS depth profile for ³¹ p ⁺ ion implanted at 5 KeV, 2.5 x 10 ¹⁵ atom per cm ² . Substrate resistivity ~0.3 ohms-cm boron doped.....	46
23.	Laser scanning of highly damaged surface laser annealed at 1.3 J/cm ² , 70% overlap factor (B9-#4). Heavy recombination at the center of overlapped area is clearly revealed.....	47
24.	Baseline process. 5.2" diameter, p type (boron doped) 0.3 ohm-cm Cz silicon.....	50
25.	Preliminary laser process. 5.2" diameter, n type (phosphorus doped) 0.3 ohm-cm Cz silicon.....	52
26.	IPEG coefficients for JPL sample process sequence.....	57
27.	Program schedule.....	64

1.0 INTRODUCTION AND SUMMARY

The objective of this contract is to develop a solar cell process sequence that incorporates three process steps which use pulsed excimer lasers, to verify that this sequence yields high efficiency cells at a low cost, and to document the feasibility of carrying this technology from the laboratory bench scale to factory size. The three process steps are: junction formation, surface passivation, and front metallization. This effort is to take place during a one-year period. The first quarter accomplishment targets the completion of 25 2x2 cm² cells of 16.5% efficiency measured at AM1.5 insolation.

This quarterly report summarizes the technical progress made since the contract initiation date of May 4, 1984.

During this reporting period, a series of annealing experiments were conducted. Parameter variations included beam energy density, percentage of beam overlap, sources of diffusant, and various surface conditions including chemical-mechanical polish, caustic etch, and texture. Diffusant deposition included spin-on liquid dopant and ion implant.

Due to the lower surface reflectivity and the "wetting" effect by the spin-on source, textured wafers are believed to experience more surface damage and stress than polished wafers. Maximum cell efficiency obtained for Cz polished wafers was 9% and for Cz textured wafers was 11.5%, without antireflection (A/R) coating. Surface damage appears to limit the cell efficiency in both cases.

Laser annealing of ion-implanted wafers was first conducted for phosphorus implants with acceleration energy of 10 keV at fluences of $1-5 \times 10^{15}$ atom/cm². Maximum cell efficiency obtained had been less than 8% (no A/R coating). The low J_{sc} , V_{oc} , and fill factor suggested incomplete implant damage removal.

By decreasing the implant voltage from 10 keV to 5 keV while increasing laser energy to above 0.9 J/cm², cell efficiency over 9.4% was obtained before A/R (13.7% after A/R). The goal of producing cells of 16.5% has not materialized due to problems of ion implant nonuniformity, unavailable low keV ion implant sources, and laser beam inhomogeneity.

Ion implantation as the dopant source is still being investigated to produce high-efficiency cells because of its potential for a high purity, tailored junction.

This quarterly report includes work for both ion-implanted and spin-on dopant sources. The two important factors for experimentation are laser energy density and overlap. The set of variables and their permutations to be investigated originally included surface conditions (texture vs. chemical polish), dopant sources, laser energy density, and overlap ratio, none of which

is independent of the others.

As yet, neither a comprehensive model nor a complete experimental matrix has been established that covers all of the issues that must be addressed in developing a viable low cost, high efficiency solar cell. At this stage we will draw on relevant segments of the literature combined with our results to piece together an empirical model that explains and will serve to guide the laser annealing experiments being conducted.

2.0 **PROGRESS**

2.1 **DEVELOPMENT OF PROCESS SEQUENCE SELECTION**

The laser process sequences investigated in the first part of the program are schematically shown in Fig. 1.

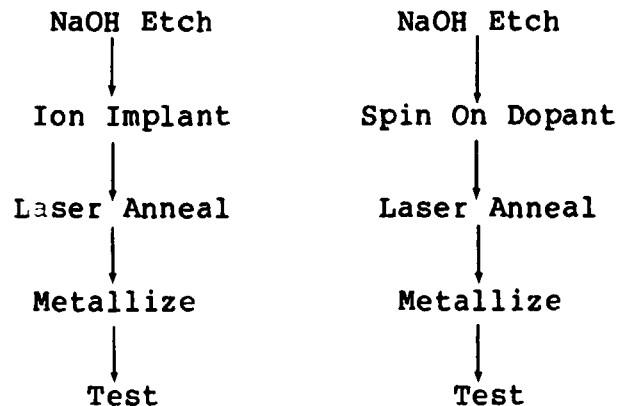


Fig. 1. Laser annealing process sequences for the First Quarter.

There were two parallel processes in the early stage of the program: one with ion implantation as the dopant source, the other with spin-on liquid dopant. P-type substrates grown by ARCO Solar were predominantly used because of their availability and their well-characterized properties. Both n-type and p-type Czochralski substrates were used based on 3-in. and 4-in. round slices as well as 4-in. squares. Floatzoned material had also been used as control samples occasionally.

After a series of experiments using liquid dopant sources without promising results, the process was discontinued. Instead, ion implantation has been substituted for N⁺ deposition on mechanically polished wafers as baseline experiments.

Optimized laser annealing parameters have been derived by an iterative method. Variables include energy density, pulse duration time, beam uniformity, and substrate temperature. Wafer cleaning and cell fabrication follow conventional methods, such as organic solution rinses, acid rinsing, and evaporated contacts.

In the later stages of the program, laser-assisted pattern writing for front grid lines and surface oxide growth for passivation will be investigated. The second phase of the laser annealing process is shown in Fig. 2.

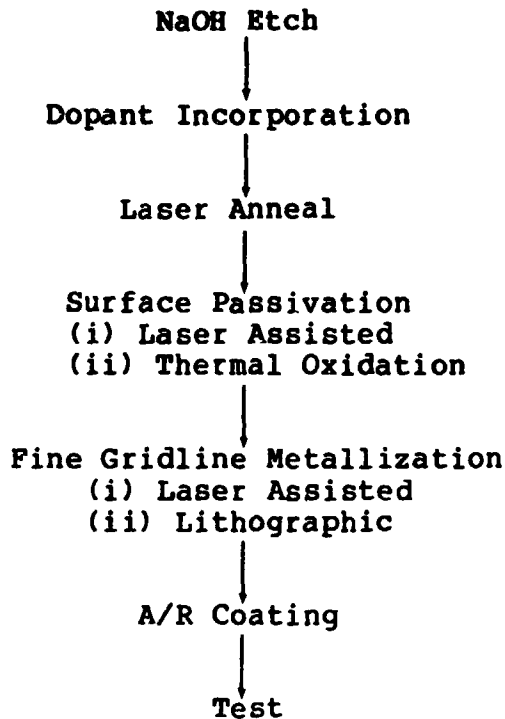


Fig. 2. Second phase process sequence.

2.2 LASER EQUIPMENT

2.2.1 Small Scale Laser

2.2.1.1 Optical System

The optical system used for laser annealing of silicon wafers by the small scale EXCI-LITE-1 laser is shown in Fig. 3. The laser source, optical train components, x-y motorized stage, and ancillary components are located on a 3x8-ft table with magnetic top surface. The optical component holders are secured to the table with magnetic bases.

The laser source is an EXCI-LITE-1 excimer laser which produces 4-20 nsec (FWH) wide output pulses with repetition rates of up to 200 Hz. The present output wavelength is 308 nm and the average laser output energy per pulse is 13-20 mJ. No pulse drop-outs have been observed in over 10^6 shots. The output beam has a square cross section of 0.8 x 0.6 mm. The light output is essentially incoherent and thus interference effects at the work surface are absent. The beam divergence is approximately 10 mrad full angle.

Adjustment of the pulse output duration was achieved by variation of the gas mixture. Figure 5a shows the temporal pulse profile using a gas mix of 0.2% Xe, 0.015% HCl with a buffer gas of He at

50 psig. A width of approximately 6 ns is observed. Upon substitution of Ne for He, the double pulse shown in Fig. 5b is observed. Such a pulse format will affect the surface annealing process more like a long pulse of duration ~20 ns.

The output beam is steered to the proper height with the beam elevator consisting of mirrors M1 and M2 shown in Fig. 4. The mirrors are coated with a dielectric multilayer stack selected for high reflectivity and independence of reflectivity with polarization at the design wavelength and angle of incidence (45°). Thus the originally unpolarized light remains unpolarized. An optional square aperture may be placed between the laser and the subsequent optical elements to create an image at the work surface with sharp edges. Aperture insertion loss is 20-50%, depending on aperture size. The light is directed to an overhead support stand (not shown) which holds lenses L1 (focal length [f.l.] = 35 cm) and L2 (f.l. = 10 cm) as well as the 90° bending mirror M3. The spacing between L1 and L2 may be varied, thus changing the effective focal length of the combination. The distance of L2 from the work surface can be adjusted, which allows variation of the image size at the work surface and permits variation of the energy density of the laser. This density may also be varied in a controlled manner by inserting neutral density filters (not shown). Lens L2 is moved axially in a coarse manner along tracks cut into the support stand, and is mounted on a precision translation stage to permit fine focal length adjustments. The overhead 90° bending mirror M3 is also angularly adjustable to allow proper centration of the light through L2 and ensure that the light is normal to the wafer surface. After proper alignment and positioning of all optical components the optical throughput is ~66% (without aperture), the main losses occurring at the four uncoated surfaces of lenses L1 and L2. The overhead support structure includes two separate, independent stations for steering mirrors and lenses. The second station (not shown) can hold optics for a second laser annealing station.

The two-stage motorized x-y annealing platform is located directly beneath the overhead optical support stand. It may be positioned below either of the two optical stations using a unislide. The motorized stages execute excursions up to 6 in. and 4 in. respectively in the x-y directions at table speeds of up to 1 in./sec. The wafer is held securely in place with an aspirator-based vacuum chuck system. Vapor and dust from the annealing process are removed by a vacuum system. The glass plate is used as the top surface on the wafer holder table and used for processing wafers up to and including the edge, thus eliminating any wasted material. The entire x-y stage and wafer holder are enclosed in a Plexiglas box to exclude dust during the processing. A gas purge of the wafer surface is employed during the processing to reduce the chance of foreign material being deposited on the surface during annealing.

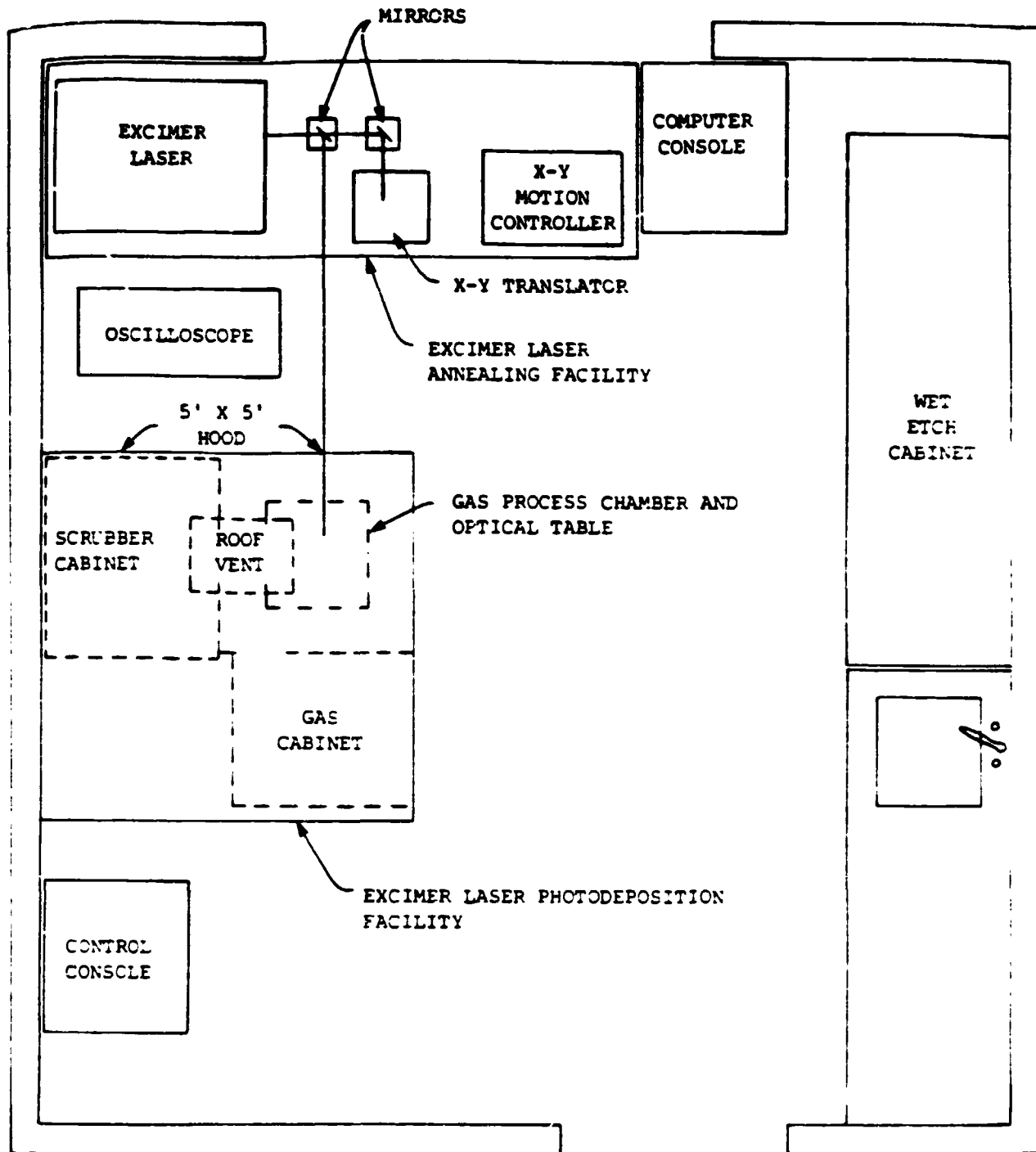


Fig. 3. Laboratory Arrangement for Excimer Laser Processing of Silicon Solar Cells.

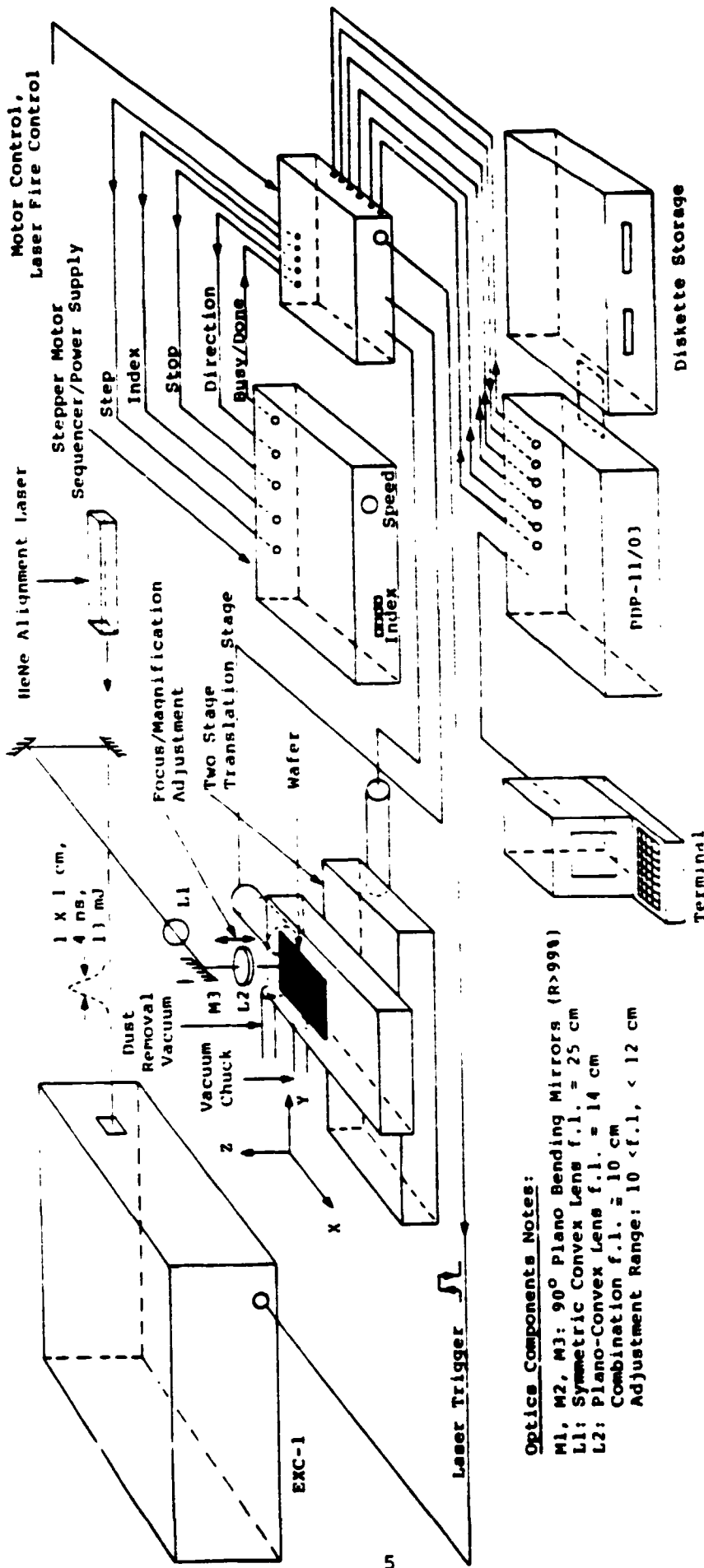
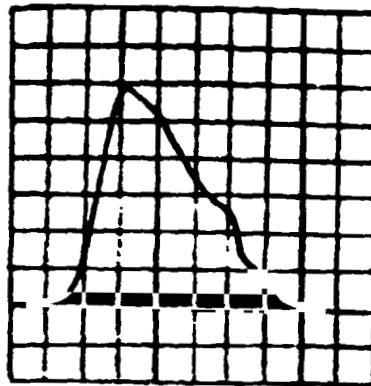
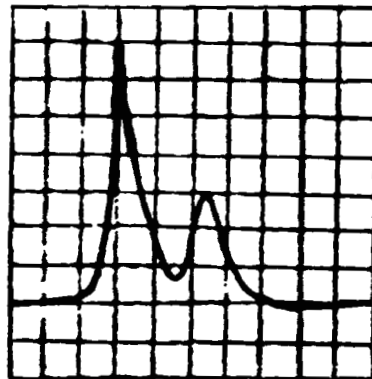


Fig. 4. Excimer Laser Annealing Facility.



2 nsec/Div

(a) Short Pulse Using Helium Diluent



10 nsec/Div

(b) Long Pulse Using Neon Diluent

Fig. 5. Typical Laser Pulse Shapes Used in Laser Annealing Process Studies.

2.2.1.2 Computer Control System

Both stepper motor controlled stages and the stepper motor sequencer and power supply were supplied by Daedal and were automated using an LSI-11 based computer as master controller, and appropriate electronics for control of laser triggering and table motion. The control program uses the parallel interface for I/O control of the sequence and laser firing. The control program was written in Macro-11 assembly language to optimize timing and execution speed.

The control program is capable of executing several distinct scan patterns designed around the two wafer geometrics which were laser annealed during this reporting period. The first pattern is a standard raster scan with user selectable pulse overlap in both directions. Both table speed and wafer size are also selectable. Based upon the input values of effective spot size and table speed, the computer controls and fires the laser at the correct frequency and allows for table acceleration time. The total number of scan lines required to cover a given annealed area is also computed and used to control the scan. User input to the program is over the serial interface to the terminal shown in Fig. 4. A given scan may also be aborted from the keyboard if desired. The annealed area resulting from the first scan pattern is square or rectangular. For circular wafers, to anneal as large an area as possible, a diagonal type annealing pattern (shown in Fig. 6) is employed. Such a pattern allows nearly the entire surface area of a round wafer to be used for solar cell fabrication. Control of all experiment parameters is available through the terminal. The control signals sent by the computer to the sequencer are shown in Fig. 4. A single power supply is used for both motors by multiplexing the sequencer output using relays in the control box. The current scan patterns do not require that both motors be operated concurrently, so this scheme is quite satisfactory.

2.2.1.3 Optical Diagnostics

Average energy measurements of the laser output as a function of repetition rate have been performed using a Scientech calorimetric type power meter. Temporal pulse width measurements were performed with a fast PIN photodiode and a 1 GHz bandwidth oscilloscope. Both widths and amplitudes showed very little pulse-to-pulse variation. A rough measurement of the transverse spatial profile using a PIN detector and a small pinhole which was moved across the beam gave qualitative results indicating non-uniformity of the transverse energy profile. More refined beam profile equipment is being developed to improve the latter diagnostic (see Section 2.2.3).

2.2.2 High Energy Excimer Laser (Lucy)

A second laboratory contains a high energy x-ray preionized excimer laser that also is being used for experiments on laser

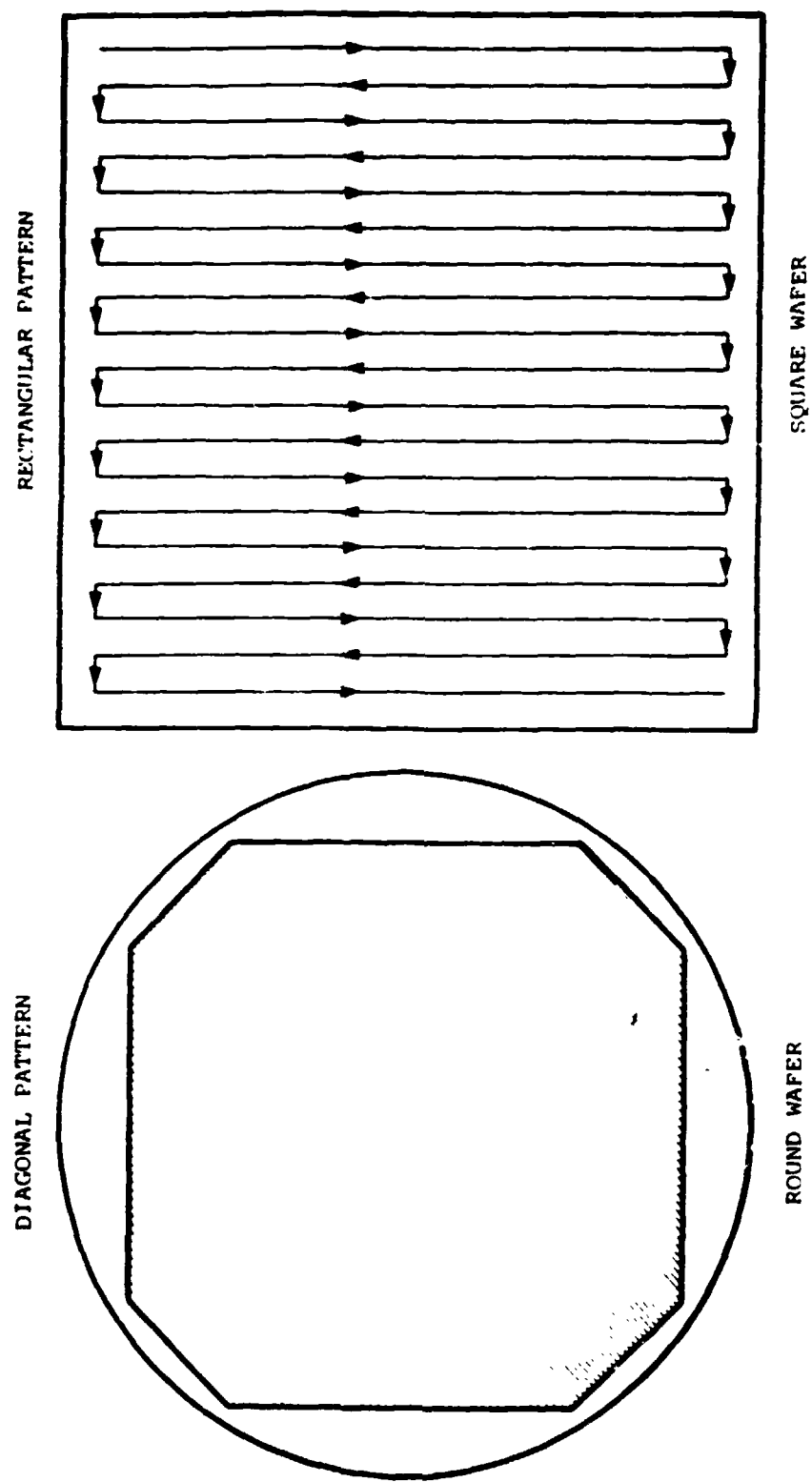


Fig. 6. Scan Patterns.

annealed junction formation. The laser was designed for experimental research on various excimer lasers, and has been adapted to the present laser annealing experiments with minimal changes.

The laboratory set-up is shown schematically in Fig. 7. The laser and energy storage supplies occupy the central area of the room. The control panels and screen room for diagnostics are located well away from the regions of high voltage, high gas pressure, and high laser intensity. Regular monitoring of the x-ray generation by the device is done in order to maintain a safe working environment for personnel. The output of the laser is reimaged on the x-y translation table through a reflective mirror that permits passage and return of the He-Ne alignment laser.

The excimer laser discharge chamber is made of Lucite with aluminum electrodes. One of the electrodes is milled very thin and transmits x-rays with very little loss. An x-ray collimator is also used to provide good spatial uniformity of the x-ray flux over the full aperture of the source. The x-ray generator is a broad area, high voltage electron gun operating at about 250 kV for 500 nsec. The electrodes are pulse charged to just below the self-break voltage, and the x-ray preionizer acts as the switch, ionizing the laser gas and causing voltage breakdown. A dielectric pulse forming line then provides current to the discharge at its self-sustaining voltage for about 75 nsec.

The discharge volume is 75 cm long by 4 cm between electrodes by 3.5 cm wide. The laser chamber includes 4 in. diameter A/R coated windows at each end. An external 20 meter radius of curvature total reflector and a 30% reflective flat output coupler form the optical cavity. To provide sharp beam edges, a rectangular aperture is included in the cavity just inside the output coupler. A He-Ne laser is used to establish good alignment of the cavity mirrors with each other and with the optical axis defined by the electrodes and the rectangular optical aperture. The focusing lens is positioned to form an image of the laser aperture at the wafer, and to provide a size reduction of about 3 to 1. The lens can be adjusted axially to vary the spot size, thereby providing variation in energy density on the wafer.

Since the large laser was originally fabricated for single pulse experiments, the construction materials limit the gas lifetime. To reduce the interaction between the laser gas and Lucite walls, a Teflon liner was introduced. At present the laser output remains constant (within 10%) for about 30 pulses before requiring replacement of a portion of the gas to bring the energy back to its original value.

2.2.2.1 Motion Control and Laser Firing

The large laser processing station consists of the beam transport

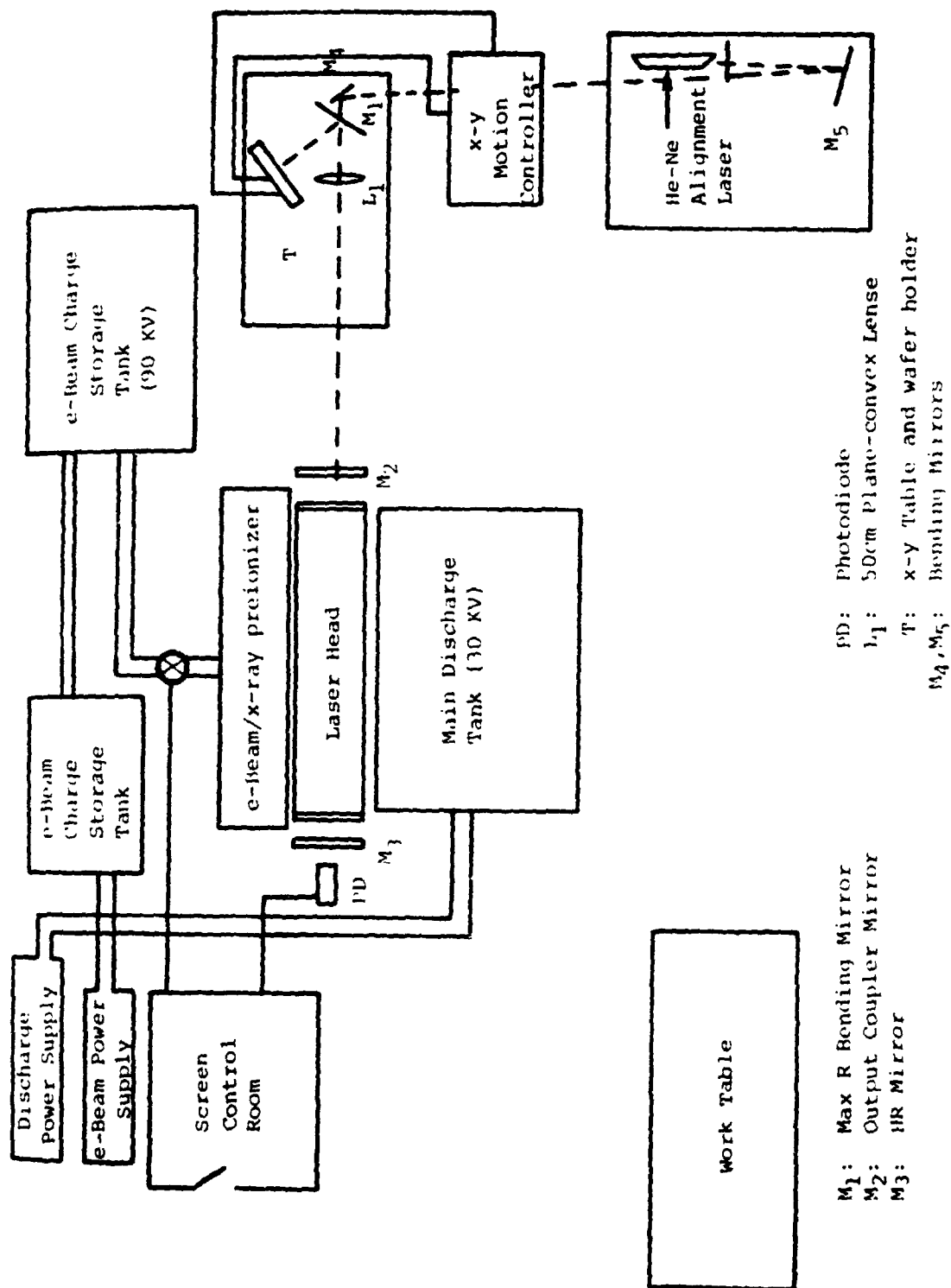


Fig. 7. Laboratory Layout for Large Excimer Laser Annealing Process.

optics as previously described and a two-axis, DC motor-driven table supplied by Aerotech. The table position is sensed by an integrated shaft encoder and direction, speed (feedrate) and position are determined by a programmable Aerotech motion controller, the Unidex III. Currently the motion controller is not interfaced to an external computer as in the case of the small excimer laser processing station, and both positioning and firing of the large laser are performed manually. To avoid the possibility of electronic damage to the controller during the high voltage electrical discharge of the large laser, the controller is turned off during laser firing. The battery backed-up internal memory of the controller permits the operator to return the table to the last position processed and then to advance to the next area to be annealed. It should be noted that in the future these steps could be automated as in the case of the small laser processing station described in Section 2.2.1.

2.2.2.2 Optical Diagnostics

A volume absorption calorimeter is used to determine pulse energy from the laser. The intensity distribution and spot size are determined by using photosensitive paper and by examining the surface of wafers that have been processed by a single spot. The pulse duration is monitored on each pulse by a fast response photodetector viewing the signal transmitted by the total reflector. A typical pulse is shown in Fig. 8.

2.2.3 Reticon Array for Beam Profiling

During this quarter a reticon array with associated frame digitizing features was developed, tested, and used to determine the characteristics of two optical beam homogenizers. In the current configuration, the reticon diagnostic digitizes and stores light intensity data at the rate of ~400 kHz. The array is designed to be used to characterize short time duration (compared with the frame time) pulses typical of excimer lasers used for laser annealing. These arrays are particularly useful for studying light intensity distributions in the UV regime since they possess a quartz window and adequate wavelength response to 0.2 μm . This is in contrast to their major competitor, CCD arrays, which typically respond only to wavelengths greater than 0.4 μm .

The array consists of 32x32 individual pixels spaced on 100 μm centers. Each individual photodiode current is stored on an integrated capacitor and read out (through an integrated shift register) every 4 msec, thus zeroing the array. By initiating the triggering of the excimer laser on the end-of-frame signal provided by the reticon array, a single shot of video information, representing the laser pulse, may be collected. Since the PDP-11 computer cannot digitize and store information at the high speeds required to minimize array dark count, a special timing and digitizing board was designed around an AMD6108 8-bit A/D (1 MHz maximum rate) and fast (150 nsec) video

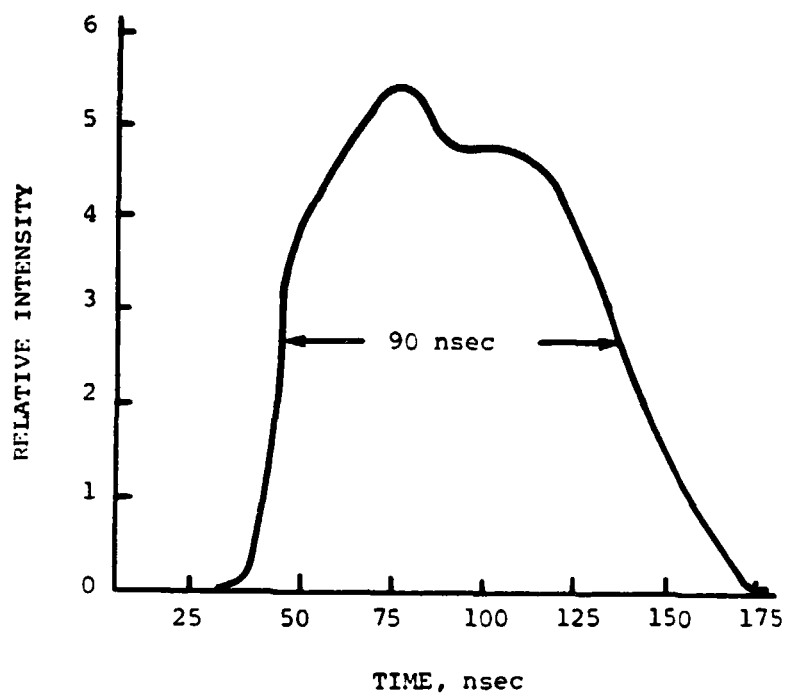


Fig. 8. Intensity Versus Time From Large X-Ray Preionized Excimer Laser Using XeCl at 308 nm.

memory. The current amount of video memory is sufficient to store 8 successive frames of spatial intensity information. The individual photodiodes have a dynamic range (manufacturer's data) of nearly 2000:1; thus the sensitivity of the array is limited by the 1 bit quantization error (measured) of the A/D converter. Thus ~0.5-1% sensitivity is possible.

During the testing phase of the array, dark count data were collected and stored in a data file. These data were then averaged and used to subtract the dark count from the actual laser beam intensity profile. The pixel-to-pixel variation in response was tested by uniformly illuminating the array with a diffuse light source. The resulting variation was less than 5%. These data were also stored to provide appropriate response scaling if desired. This information is then transferred to a PDP-11 computer and saved in a diskette data file. The information is then transferred to a VAX 11/780 computer where a Gaussian curve fit routine may be used to extract pertinent information on the spatial size and ellipticity of the pulse. Also, a contour plotting routine may be employed to give direct visual information concerning the two dimensional energy distribution. Such information is shown in Fig. 9 which is the output of a small HeNe laser. The output is Gaussian as expected, and the profile was found to be slightly elliptical.

To characterize the optical kaleidoscope to be used for beam homogenization of the EXCI-LITE-1 laser, the same HeNe beam was used to test the performance of the kaleidoscope, as well as the influence of the $f/\#$ (which determines the number of internal reflections) of the input optics on the uniformity of the output beam. The first optical set-up is shown in Fig. 10. To closely approximate the behavior of the excimer laser, the small HeNe ($W_0 = 0.45$ mm) beam was expanded in the telescope consisting of a 25 mm lens followed by a 250 mm lens. The resulting beam was then focused into the kaleidoscope using the 40 mm lens shown. The $f/4$ input optics resulted in the fairly uniform beam shown in Fig. 11. This profile was taken at the output of the kaleidoscope and measured 3x3 mm. To test our ability to reduce this object size to an image size compatible with our desired energy density at the work surface, an $f/1$ optic was used at a 2:1 conjugate ratio with the resulting image shown in Fig. 12. The image is both square and possesses a rapid drop-off in intensity at the edges. The uniformity of the beam could be improved over that shown in Figs. 11 and 12 if the input and output faces of the kaleidoscope were better polished. An imperfection in at least one of the faces was observed to lead to spurious light scattering. The conclusion from this experiment is that $f/4$ input optics are sufficient to homogenize the beam to the $\pm 7\%$ level. Figure 12 indicates that beam overlapping of 100-200 μ m at the work surface should be sufficient.

In another series of experiments the 5x5 mm kaleidoscope was used with the identical optical train. The resulting output was too large to record in a single shot on the reticon, but by scanning

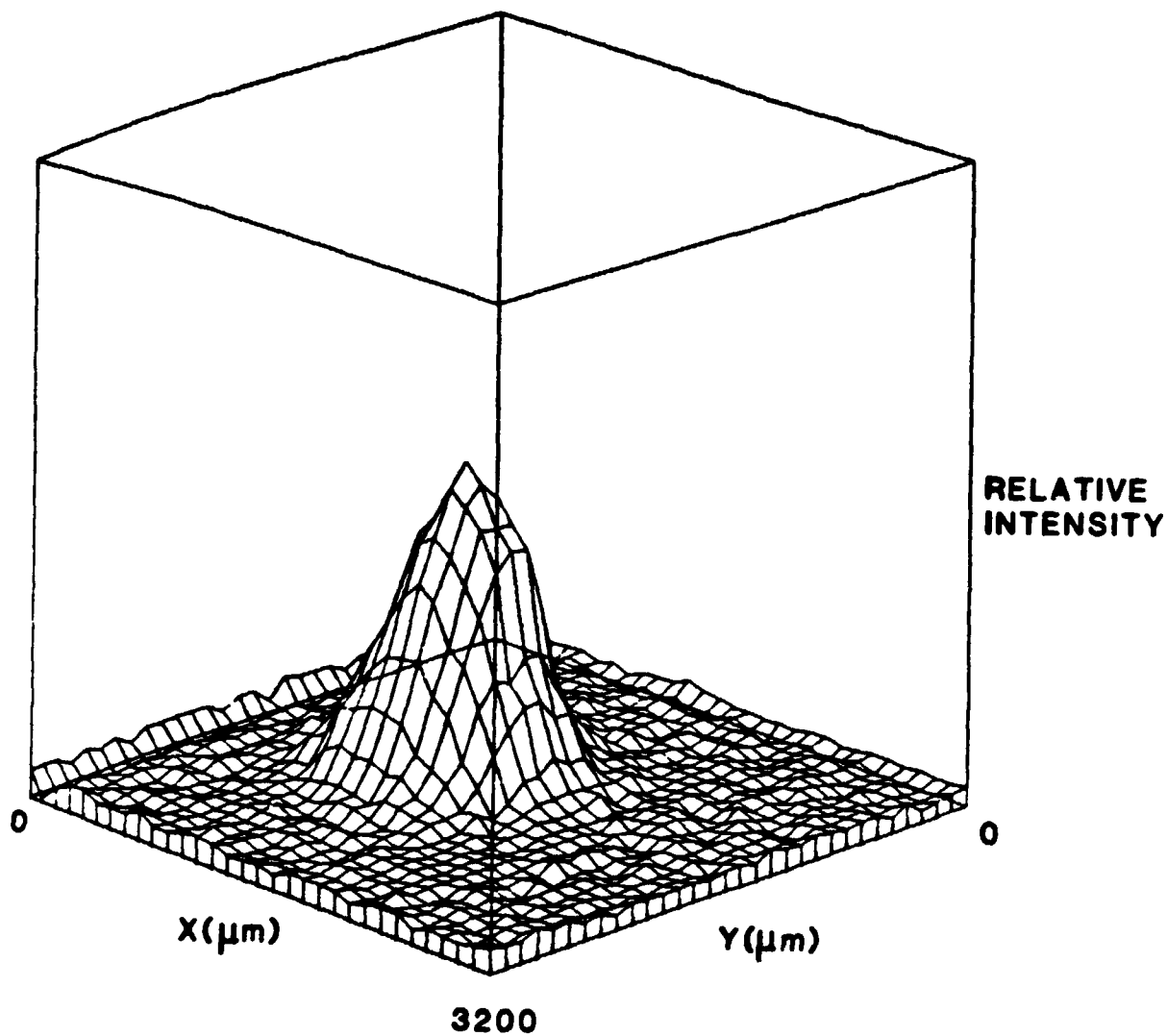
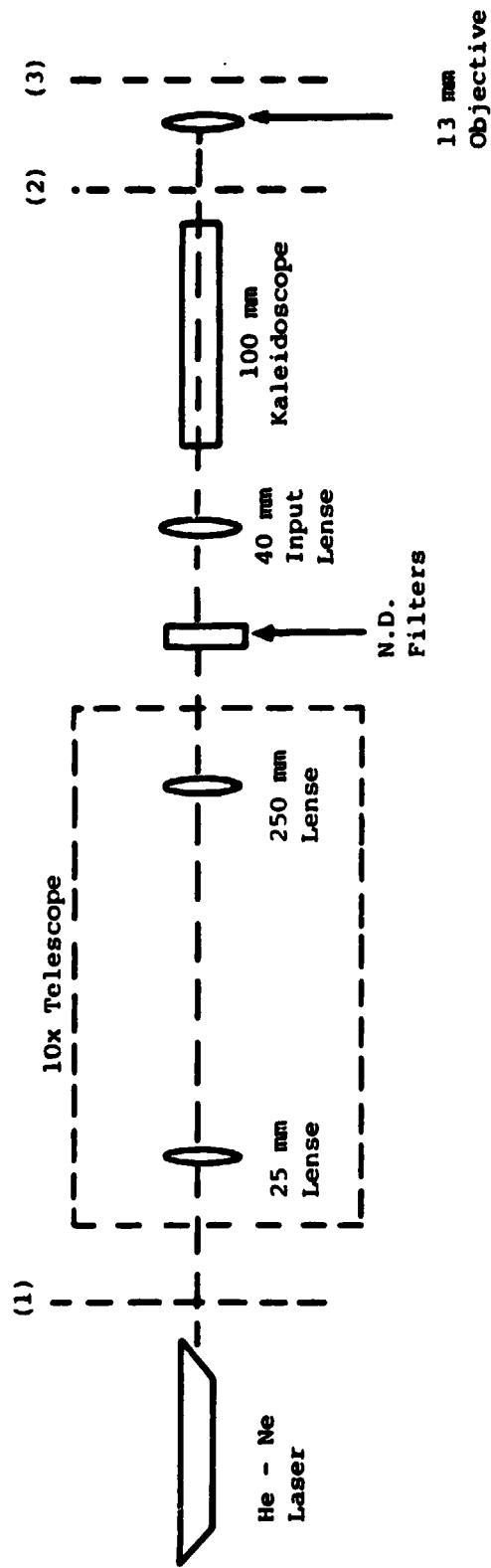


Fig. 9. Input He-Ne Beam Used for Testing Kaleidoscope Beam Homogenizer.



Notes:

(1), (2), (3): Reticon Imaging Locations

Fig. 10. Optical Set-Up for Kaleidoscope Testing.

the array across the optical field the output (using f/4 input optics) was found to be as uniform as that shown in Fig. 8 for the 3x3 mm kaleidoscope. The difficulty with the 5x5 mm kaleidoscope stems from the large size reduction ratio required to achieve energy densities of $\sim 1.2 \text{ J/cm}^2$ at the work surface. Thus, although the 5x5 mm kaleidoscope is of superior optical quality, it is not suitable for the EXCI-LITE-1 at present. Recently three 2x2x100 mm kaleidoscopes of better optical quality were ordered. f/1 optics will be used to reduce the image size to about 1 mm square. The new kaleidoscopes will have beveled edges to prevent chipping during the polishing process, and will have a high polish on all six surfaces. This will then require a laser energy of 12 mJ at the work surface. Since 60-70% of the input light is present at the kaleidoscope output, the required laser output energy is $\sim 20 \text{ mJ}$.

It was found that with careful alignment and optimization using the reticon array diagnostic, even fewer internal reflections (such as provided by f/6 optics) can yield sharp edges and good beam uniformity (see Fig. 13). The picture in Fig. 11 was taken with the image slightly offset from the center of the reticon to illustrate the sharp intensity gradient at the edges. This is an obviously desirable characteristic with regard to successful laser annealing of silicon wafers.

In a recent set of experiments, the actual output beam (suitably attenuated) of the small excimer laser previously described in Section 3.1 was characterized by the reticon array. Figure 14 shows the resulting profile of the beam. The intensity was reduced 10^7 using N.D. filters and then the spot was reduced to $\sim 2 \times 2 \text{ mm}$ using a single simple 250 mm lens. In addition, several other independent profiles at the identical image plane were taken to determine shot to shot variation in energy distribution. It was found that although the energy centroid remained approximately constant, intensity spikes occurred which are undesired, and will be removed by beam homogenization.

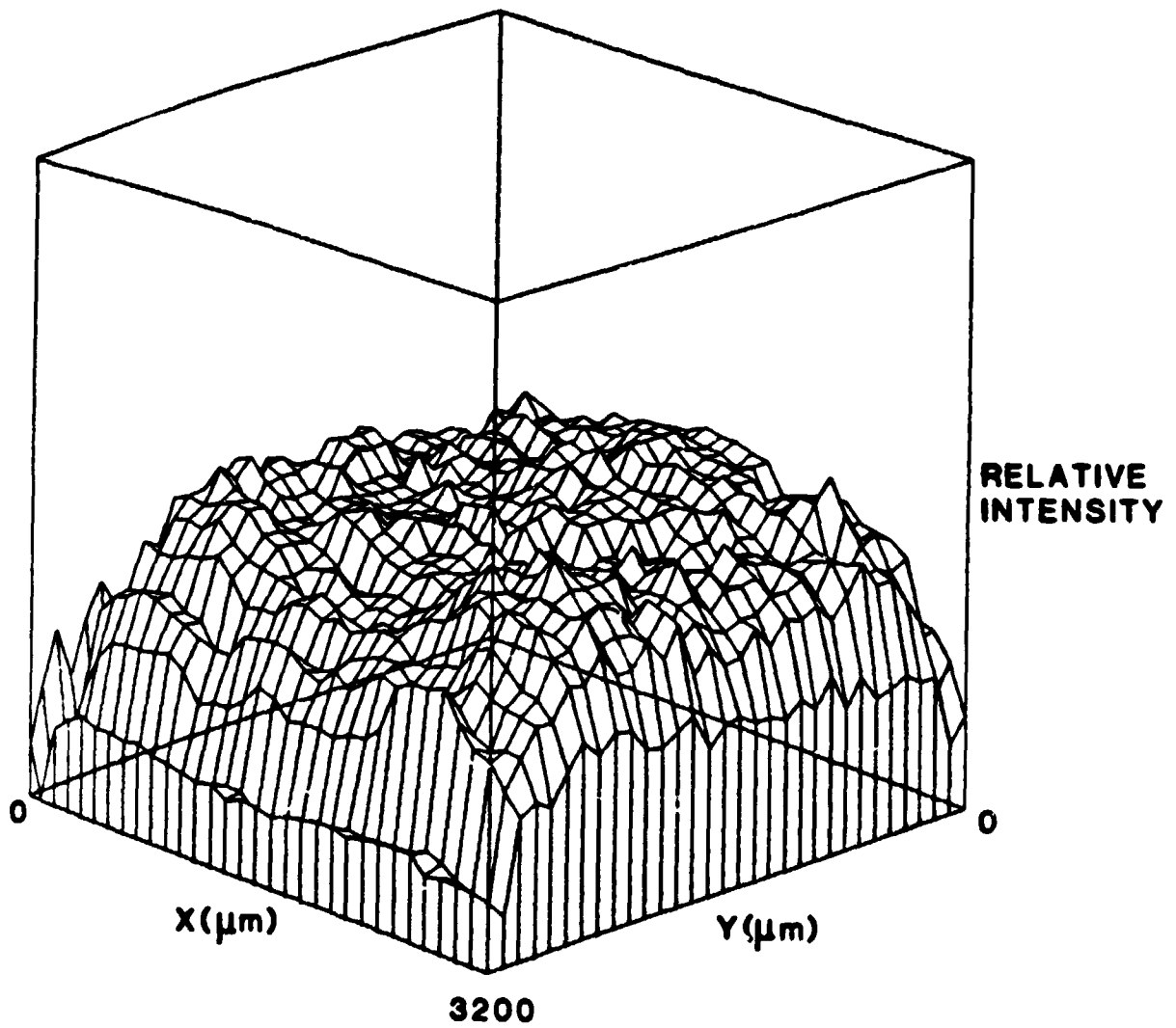


Fig. 11. Beam Profile at Exit Plane of Kaleidoscope Using $f/4$ Input Optics.

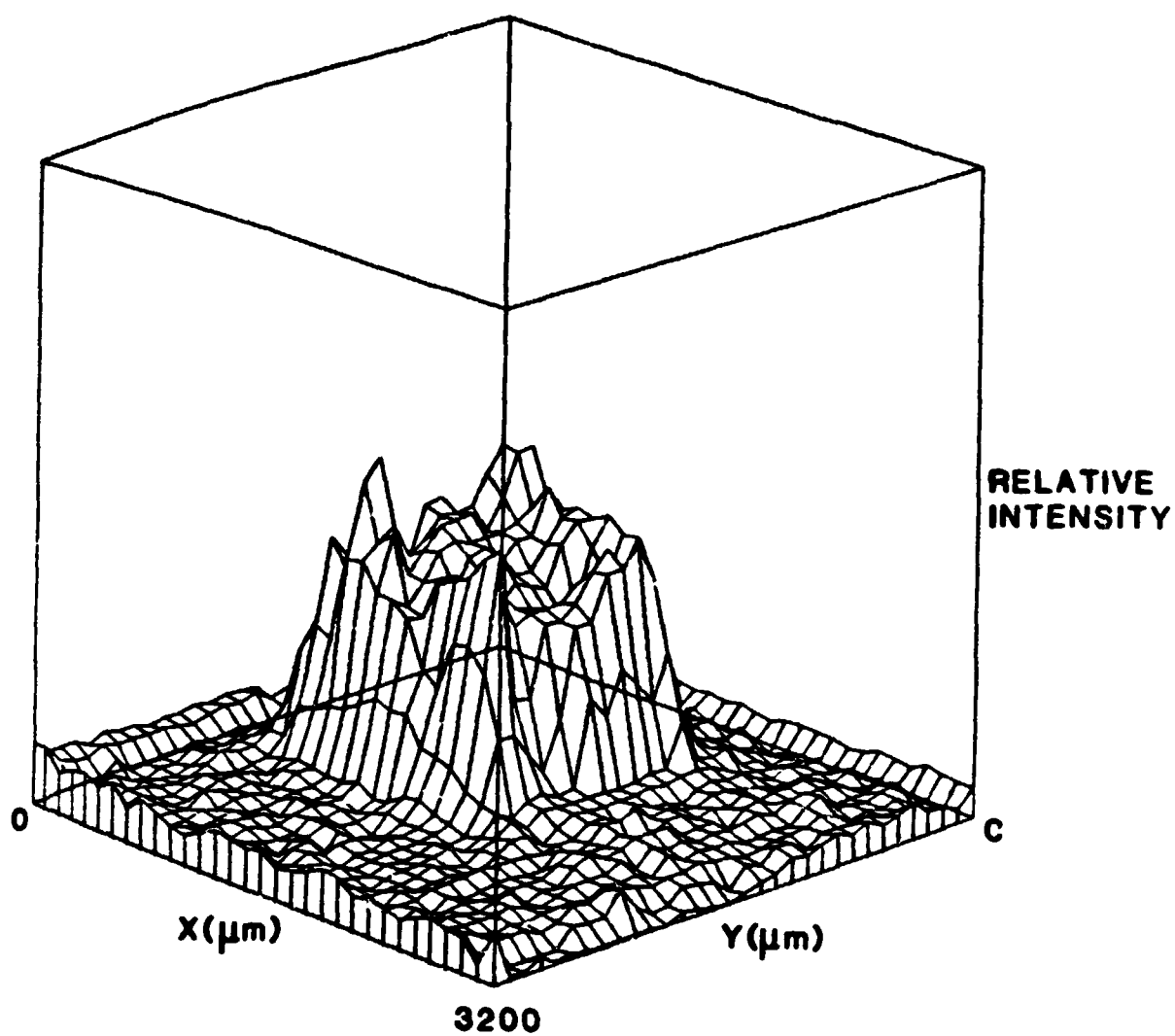


Fig. 12. Beam Profile Demagnified 2x and Reimaged.

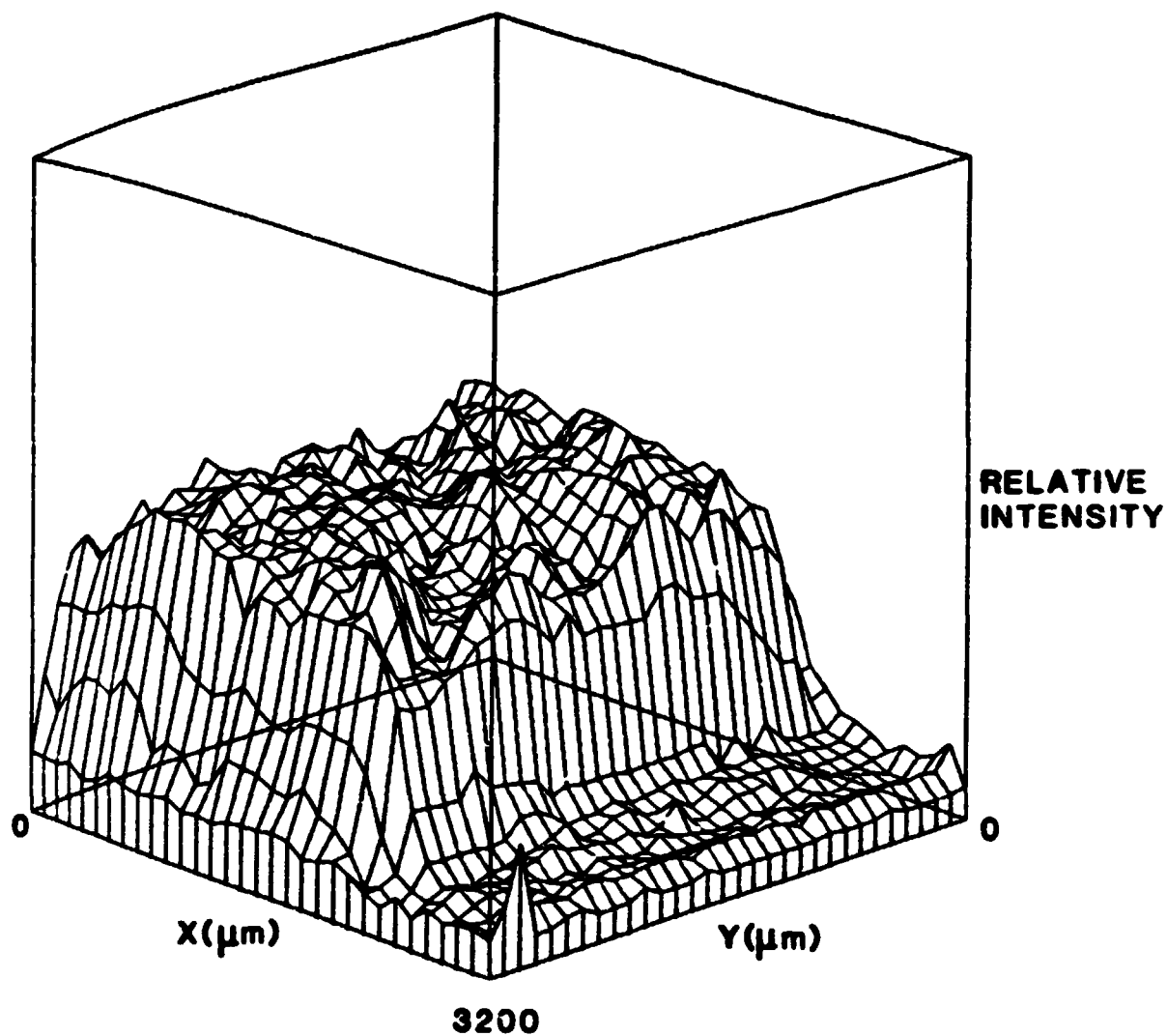


Fig. 13. Beam Profile at Exit Plane of Kaleidoscope Using f/6 Input Optics.

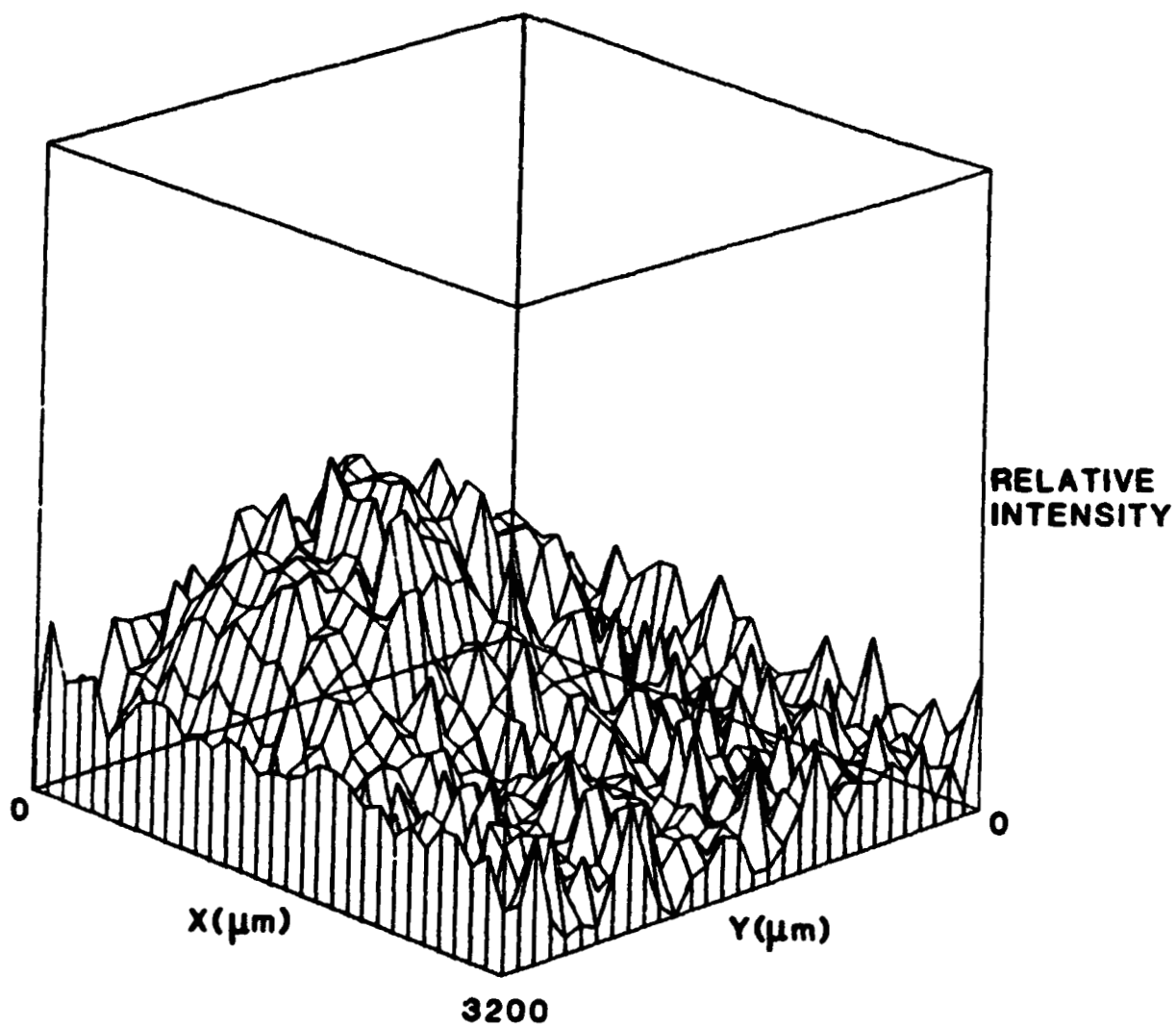
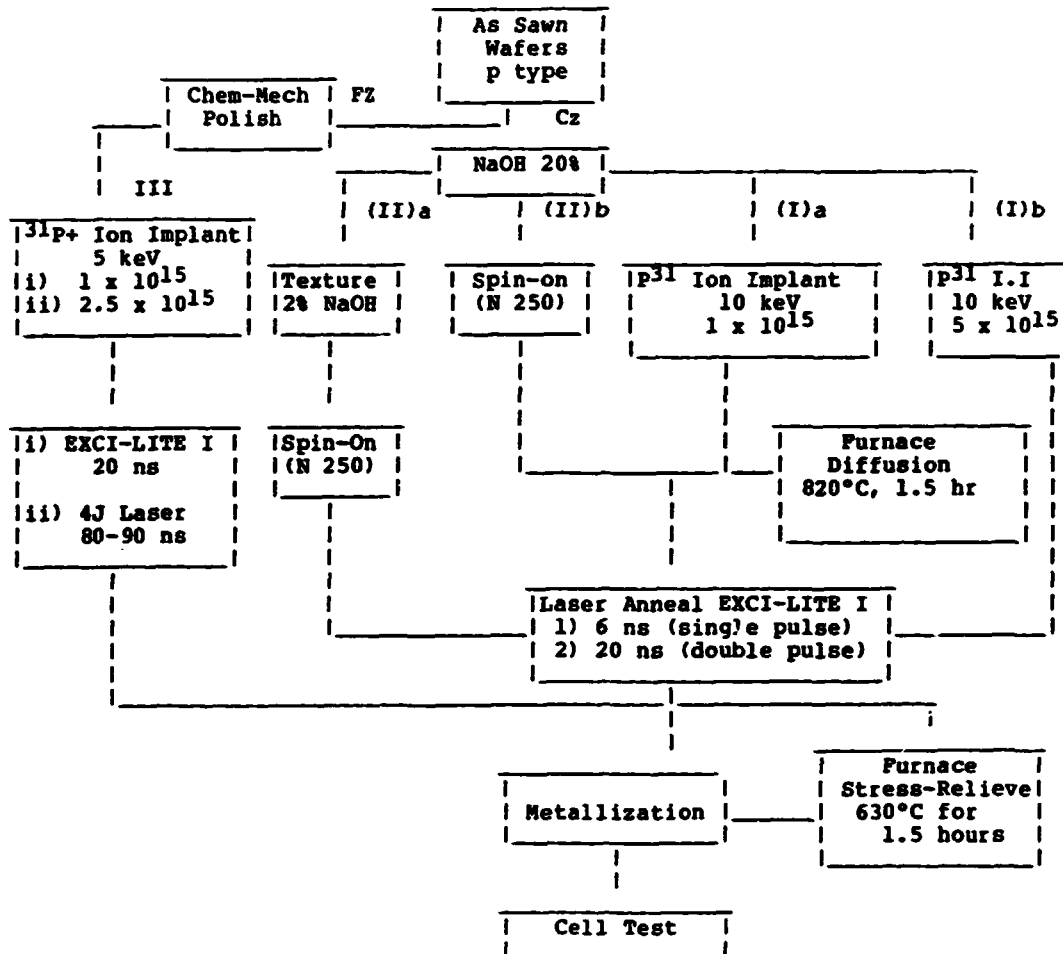


Fig. 14. Profile of Excimer Output Beam.

2.3 QUARTERLY ACTIVITIES

Figure 15 describes the quarterly activity.



- i) Starting material included Cz, both texturized and caustic etched, and FZ which was chem-mechanically polished.
- ii) Emitter dopants of spin-on source were Emulsitone N250 and Allied Chemical PX-10 respectively.
- iii) 31P+ ion implantation at 10 keV and 5 keV with 1, 5, 2.5x10¹⁵ atoms/cm² fluence respectively.
- iv) Laser used had been EXCI-LITE 1 (small XeCl laser) and "Lucy" (large 4 J laser).
- v) Metallization has been by shadow mask evaporation method, with 92% active area. Lithography will be applied in the 2nd quarter.

- vi) Cells were tested at direct AM1.5 with SERI calibrated cell Y128 which was found identical with the reference cell provided by JPL #MT-472.
- vii) Sequence of experiments with various laser parameters and implantation are summarized in Table 1.

Table 1

EXCIMER LASER ANNEALING PARAMETERS

Wafer Type	Batch No.	Date, 1984	Laser Energy MJ	Spot Size, mm x mm*	Average Energy Density, J/cm ²	Pulse Duration, nsec	Table Speed, cm/sec	Spot Interval, mm x mm*	Overlap, Percent*	Laser PRP, sec ⁻¹
Spin-On	1	May 9	5	0.6 x 0.4	2.0	4	1.2	0.4 x 0.3	30	31
	2	May 21	6	1.1 x 0.8	0.7	6	2.5	0.6 x 0.45	45	42
	3	May 25	7	1.1 x 0.8	0.8	6	2.5	0.8 x 0.6	25	31
	4	May 31	6	1.1 x 0.8	0.7	6	2.5	0.55 x 0.4	50	45
Spin-On Ion Implant	5a	June 6	6	1.1 x 0.8	0.7	6	2.5	0.55 x 0.4	50	45
	5b	June 6	5	1.3 x 1.0	0.4	6	2.5	0.4 x 0.25	70	65
	5c	June 6	4	0.8 x 0.6	0.8	6	2.5	0.25 x 0.25	70 x 60	100
	5d	June 14	7.5	0.8 x 0.6	1.5	6	1.2	0.25 x 0.20	70	50

* First number corresponds to spot dimension along direction of simultaneous table travel and laser firing.

Table 1 (Cont.)

EXCIMER LASER ANNEALING PARAMETERS

Wafer Type	Batch No.	Date, 1984	Laser Energy mJ	Spot Size, mm x mm*	Average Energy Density, J/cm ²	Pulse Duration, nsec**	Table Speed, cm/sec	Spot Interval, mm x mm*	Overlap, Percent*	Laser PRP, sec ⁻¹
Spin-On Ion Implant	5a	June 6	6	1.1 x 0.8	0.7	6	2.5	0.55 x 0.4	50	45
	5b	June 6	5	1.3 x 1.0	0.4	6	2.5	0.4 x 0.25	70	65
	5c	June 6	4	0.8 x 0.6	0.8	6	2.5	0.25 x 0.25	70 x 60	100
	5d	June 14	7.5	0.8 x 0.6	1.5	6	1.2	0.25 x 0.20	70	50
Spin-on Ion Implant	6a	June 22	11	1.0 x 0.9	1.2	25	2.5	0.5 x 0.45	50	50
	6b	June 22	11	1.0 x 0.9	1.2	25	2.5	0.5 x 0.45	50	50
Spin-on and Etched	7a	June 27	9	1.0 x 1.0	0.9	25	2.5	0.5 x 0.5	50	50
	7b	June 27	11.3	1.0 x 0.95	1.2	25	2.5	0.5 x 0.5	50	50
	7c	June 27	11.3	0.9 x 0.8	1.6	25	2.5	0.45 x 0.4	50	55
Spin-on and	8a	July 3	12	1.3 x 1.3	0.7	25	2.5	0.4 x 0.4	70	62
	8b	July 3	12	1.7 x 1.6	0.44	25	2.5	0.5 x 0.45	70	50
Textured	8c	July 3	10	1.7 x 1.6	0.36	6	2.5	0.5 x 0.45	70	50

* First number corresponds to spot dimension along direction of simultaneous table travel and laser firing.

** The 25 nsec laser pulse was composed of 2 pulses spaced 25 nsec, each having a FWHM duration of 6 to 10 nsec.

Table 1 (Cont.)
EXCIMER LASER ANNEALING PARAMETERS

Wafer Type	Batch No.	Date, 1984	Laser Energy mJ	Spot Size, mm x mm*	Average Energy Density, J/cm ²	Pulse Duration nsec**	Table Speed, cm/sec	Spot Interval, mm x mm*	Overlap, Percent*	Laser PRF, sec ⁻¹
5 keV Ion	9a	July 13	12	.95 x .95	1.3	25	2.5	0.3 x 0.3	70	77
Implant	9b,c	July 13	11	1.2 x 1.0	0.9	25	2.5	0.4 x 0.3	70	62
Ion	10a	July 25	5.6	0.85 x 0.7	0.9	25	2.5	0.6 x 0.5	30	42
Implant	10b	July 25	5.6	0.75 x 0.6	1.25	25	2.5	0.6 x 0.5	20	42
Spin-on	10c	July 25	5.4	0.75 x 0.6	1.2	25	2.5	0.6 x 0.5	20	42
5 keV Ion	11***	Aug 2	900	9 x 7.5	1.3	80	--	7.2 x 6.4	20	--
5 keV Ion	12a	Aug 9	1200	9.1 x 7.7	1.65	90	--	8.4 x 6.8	8	--
Implant	12b	Aug 9	1200	9.1 x 7.7	1.65	90	--	8.4 x 6.8	8	--
5 keV Ion	13	Aug 14	1100	11.8 x 10.0	0.95	90	--	10.7 x 9.0	9	--
5 keV Ion	14a	Aug 16	1220	11.4 x 9.8	1.1	90	--	10.7 x 9.0	7	--
Implant	14b	Aug 16	1220	11.4 x 9.8	1.1	90	--	10.7 x 9.0	7	--
Thermal Implant	15	Aug 21	1200	10.3 x 9.0	1.3	90	--	9.3 x 8.0	10	--

*First number corresponds to spot dimension along direction of simultaneous table travel and laser firing.

**The 25 nsec laser pulse was composed of 2 pulses spaced 25 nsec, each having a FWHM duration of 6 to 10 nsec.

***Parameters varied over wafer. Values listed correspond to region that gave best cell.

3.0 SIGNIFICANT EXPERIMENTAL RESULTS

Results can be separated into two major categories, spin-on dopant source and ion implantation. All annealing experiments for liquid dopants were conducted with the EXCI-LITE laser with a beam spot of approximately 0.6x0.8 mm. In the early stage of annealing ion implanted wafers, the EXCI-LITE laser was also used. However, in order to obtain minimum overlap percentage and to get the best uniformity available, a more powerful 4J laser was used.

3.1 LIQUID DOPANT

The annealing experiment was started using a phosphorus spin-on dopant source on p-type Cz wafers of 0.7 ohm-cm base resistivity. Surface conditions included chemical polish and texture. Threshold laser energy was found to be different for the two due to differences in surface reflectivity as expected.

3.1.1 Textured Surface

Energy density as low as 0.4 J/cm² (70% overlap) was found sufficient to melt the texturized surface. However, cells were almost all badly shunted (Table 2a). A sister wafer (2x4 in.) that had been laser annealed at the same settings went through an additional furnace heat treatment at 650°C for 30 minutes before metallization. This cell had its efficiency improved to as high as 11.7% (Table 2b). Such low temperature heat treatment is believed to stress-relieve the melt-recrystallized surface.

Cell performance of 0.7 J/cm² annealing with 50% overlap showed further improvement. Highest cell efficiency was about 11.6% before A/R coating (Table 2c). Heat treatment to the 0.7 J/cm² annealed wafer did not show obvious improvement. A possible explanation could be that 0.7 J/cm² was sufficient to cause more complete surface regrowth with less relievable stress. In fact, SEM photographs of these two samples indicated much more surface resolidification with 0.7 J/cm² than with 0.4 J/cm² (Fig. 16).

Table 2. Textured Cz p-type wafer with spin-on source laser annealed:

a. At 0.4 J/cm² with 70% overlap.

Cell ID	V _{oc} , V	J _{sc} , mA/cm ²	FF, %	Eff, %
B5B 1	0.429	28.32	59.60	7.24
2	0.406	28.26	57.30	6.56
3	0.399	28.24	55.40	6.25
4	0.434	27.89	57.60	6.97

ORIGINAL PHOTO IS
OF POOR QUALITY.

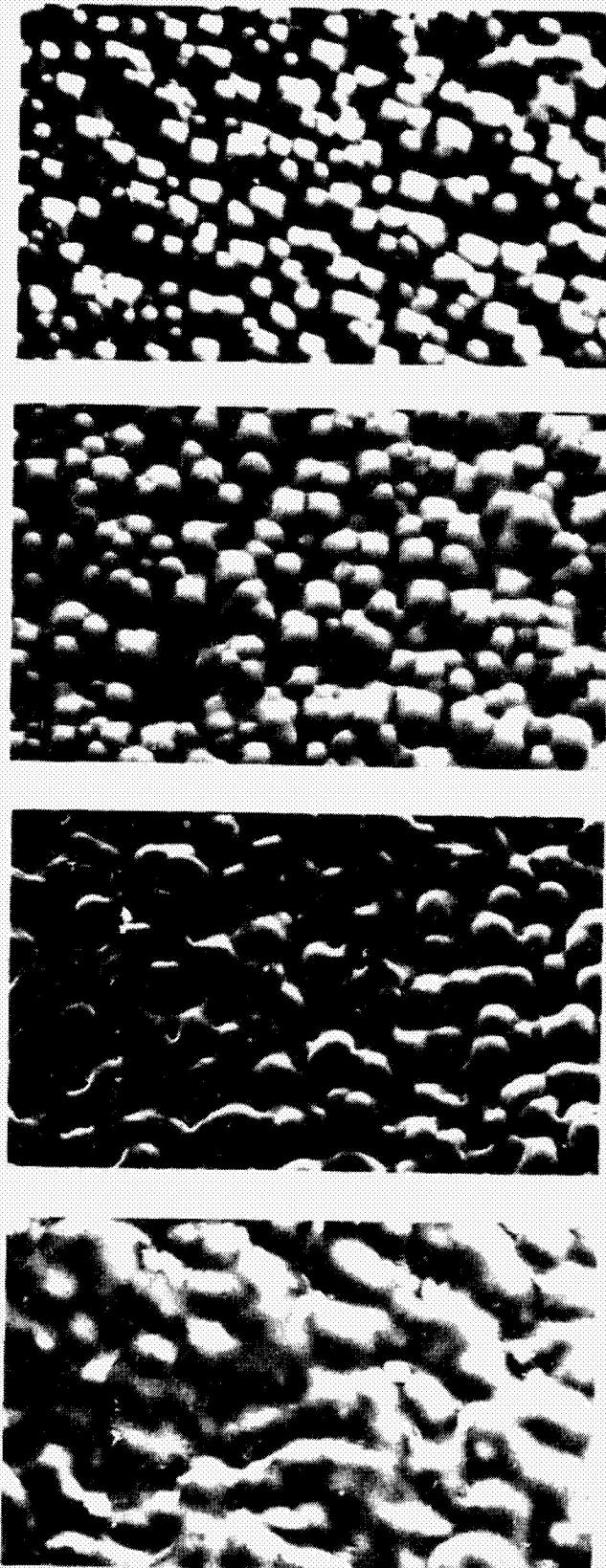


Fig. 16. 500 x SEM on Textured Wafers (With Spin-On Liquid Dopant) After Laser Annealing at (a) 0.4 J/cm^2 , (b) 0.7 J/cm^2 , (c) 1.2 J/cm^2 , (d) 2.5 J/cm^2 .

b. At 0.4 J/cm² with 70% overlap followed by furnace heat treatment at 650°C for 30 minutes.

Cell ID	V _{oc} , V	J _{sc} , mA/cm ²	FF, %	E _{ff} , %
B5BT 1	0.555	28.95	69.50	11.18
2	0.560	29.04	67.40	10.96
3	0.563	28.54	69.10	11.10
4	0.560	28.90	68.90	11.15
5	0.573	28.66	71.40	11.73
6	0.544	29.08	65.00	10.27

c. At 0.7 J/cm² with 50% overlap.

Cell ID	V _{oc} , V	J _{sc} , mA/cm ²	FF, %	E _{ff} , %
B5A 1	0.534	29.94	69.30	11.08
2	0.536	29.56	68.60	10.87
3	-	-	-	-
4	0.459	26.34	63.00	7.74
5	-	-	-	-
6	0.549	30.43	69.66	11.64

High energy density, e.g. at 1.2 J/cm², yielded lower cell efficiency (~8.7%) due to severe reduction in J_{sc} (21 mA/cm²) because of loss in texturing. SEM photos (Fig. 15c) also revealed that heavy melting-resolidification took place after such high energy density annealing. The effective energy density at the surface was increased at least by 40% due to the second reflection from the textured surface.

3.1.2 Chemically Polished Surface

In parallel with the textured wafer experiment, 20% NaOH etched wafers (Cz 0.7 ohm-cm p-type base) had spin-on liquid dopant followed by laser annealing at energy densities of 0.9 J/cm², 1.2 J/cm², and 1.6 J/cm² with 50% overlap. Results are summarized in Table 3. The data represent the average cell efficiency weighted over 4 samples in each case. Also included in Table 3 are the results of post furnace annealing at 650°C for 30 minutes to test for a stress relief effect.

Table 3. Cells fabricated from polished Cz p-type wafer with spin-on source laser annealed at energies 0.9, 1.2, and 1.6 J/cm².

Cell ID	Laser Energy, J/cm ²	Control				650°C Furnace Annealed			
		V _{oc} , V	J _{sc} , mA/cm ²	FF, %	Eff, %	V _{oc} , V	J _{sc} , mA/cm ²	FF, %	Eff, %
B7-I (1F)	1.2	0.586	20.65	75.3	9.1	0.587	19.90	76.0	8.9
B7-III (2F)	0.9	0.582	21.15	68.8	8.5	0.589	20.54	73.0	8.8
B7-II (3F)	1.6	0.588	19.40	75.9	8.6	0.587	18.60	79.7	8.5

As indicated by the data, the shallow junction formed by annealing at 0.9 J/cm² on these reflective surface wafers improved the J_{sc} in comparison with other groups (Hovel, 1975).

However, the fill factor was lowered as a result of increased series resistance. Deeper junctions of groups I and II had much better fill factor yet lower J_{sc}, confirming the statement above. It is interesting to notice that 1.2 J/cm² energy density had yielded the highest efficiency cell, which is consistent with other published articles. However, surface damage due to the "wetting" effect of the spin-on coating was most severe at 1.2 J/cm². Flow of molten silicon was obvious at 0.9 J/cm² (Fig. 17a). "Crater" defects were found on the 1.2 J/cm² annealed surface (Fig. 17b).

Furnace annealing at 650°C for 30 minutes (before metallization) improved the fill factor slightly, especially on group I (0.9 J/cm²), but degraded the J_{sc} by approximately 3-4%. The results suggest that thermal stress relief appears effective only for low laser energy density annealed surfaces, which is similar to the observation for the textured surface.

For control purposes, liquid dopant on caustic etched wafers were subjected to thermal diffusion at 820°C for 1.5 hours. Results are summarized in Table 4.

ORIGINAL PAGE IS
OF POOR QUALITY



Fig. 17a. Laser Annealing (B7-3F) at 0.9 J/cm² on Caustic Polished Surface With Spin-On Liquid Dopant Source. Heavy Melting and Surface Damage are Clearly Shown.



Fig. 17b. Pimple Type Crater Defects on Surface Annealed at 1.2 J/cm².

Table 4. Cell performance of thermally diffused wafer of caustic polished with spin-on source as dopant.

Cell ID (Cz)	V _{oc} , V	J _{sc} , mA/cm ²	FF, %	Eff, %
Spin on B5-C				
(1)	0.531	22.87	64.4	7.8
(2)	0.563	23.33	71.1	9.3
(3)	0.559	23.43	71.8	9.4
(4)	0.585	22.43	60.2	7.9
(5)	0.540	23.00	71.4	8.9

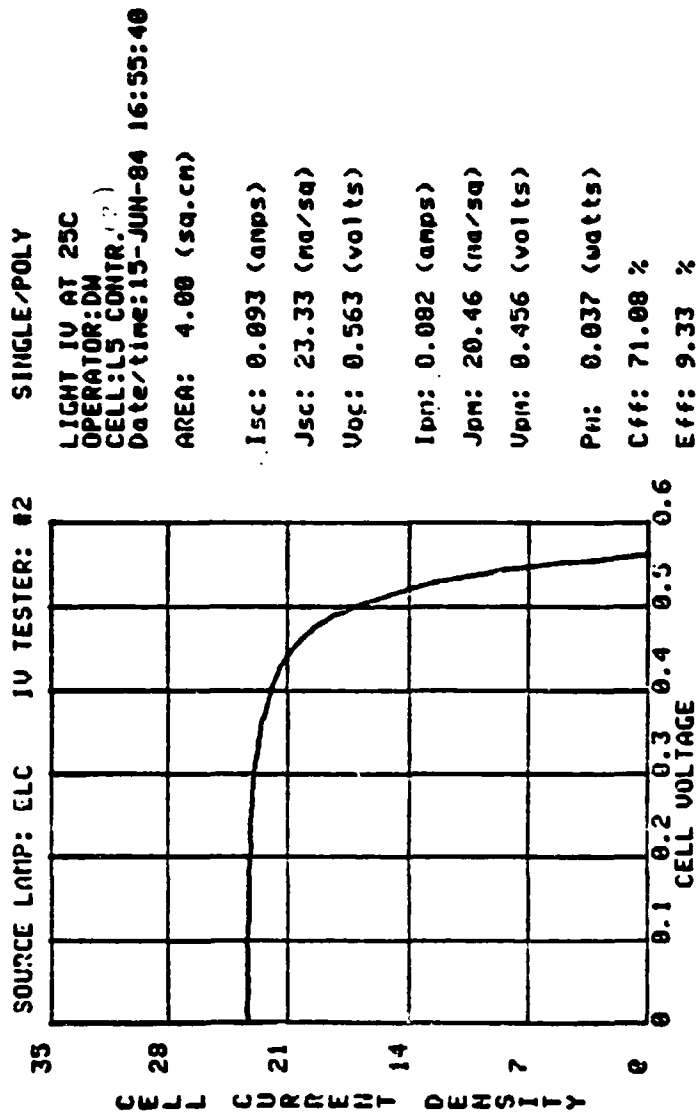
Cell efficiency of the thermally diffused wafers on average was better than those laser annealed due to higher J_{sc}, suggesting that the junction depth of thermally diffused cells with spin-on dopant was even shallower (Fig. 18a). The lower V_{oc} was probably due to high recombination in the junction as indicated by the dark I-V (Fig. 18b). In fact, all cells with emitters diffused both thermally or laser assisted with liquid dopant had high dark recombination current. One of the possible sources of recombination centers could be from the liquid dopant, as one of the supplier's analytical data showed impurity levels were as high as 0.5 ppm. The usage of liquid dopant was then halted.

3.2 ION IMPLANTED EMITTER

In the early stage of the program, ion implants were processed for 4-in. diameter p-type caustic polished Cz (~0.33 ohm-cm) wafers at 10 keV with dosage of 5x10¹⁵ atoms/cm² and 1x10¹⁵ atoms/cm² respectively. Laser energy density (EXCI-LITE-1) was set at 0.4 J/cm² and 0.7 J/cm², respectively, with pulse duration 4-6 ns. Cell characterization indicated low J_{sc}, V_{oc}, and fill factor as the result of insufficient implant damage removal by low laser energy density that was too low. Typical results are listed in Table 5.

Table 5. Results of laser annealing in caustic polished, 10 keV ion implant with dosage 5x10¹⁵ and 1x10¹⁵ atoms/cm², respectively.

Cell ID (Cz)	10 keV Ion Implant Dosage x10 ¹⁵	Laser Energy Density, J/cm ² (% Overlap)	V _{oc} , V	J _{sc} , mA/cm ²	FF, %	Eff, %	Sheet Rho, ohm/sq
B5A #5	5	0.7 (50% O.L.)	0.581	18.7	67.0	7.3	33
B5B #4	5	0.4 (70% O.L.)	0.516	18.7	64.9	6.3	31
L5A #7	1	0.7 (50% O.L.)	0.389	20.4	52.1	4.2	90
L5B #4	1	0.4 (70% O.L.)	0.479	19.8	68.3	6.5	87



SPIN ON SOURCE - AUTO POLISHED
 SINTERED
 THERMAL ANNEALED @ 820 C X 1.5 HOURS

Fig. 18a. Electrical Characteristics of a Thermally Diffused N+ Spin-On Liquid Source on P Substrate, (a) Light I-V and (b) Dark I-V.

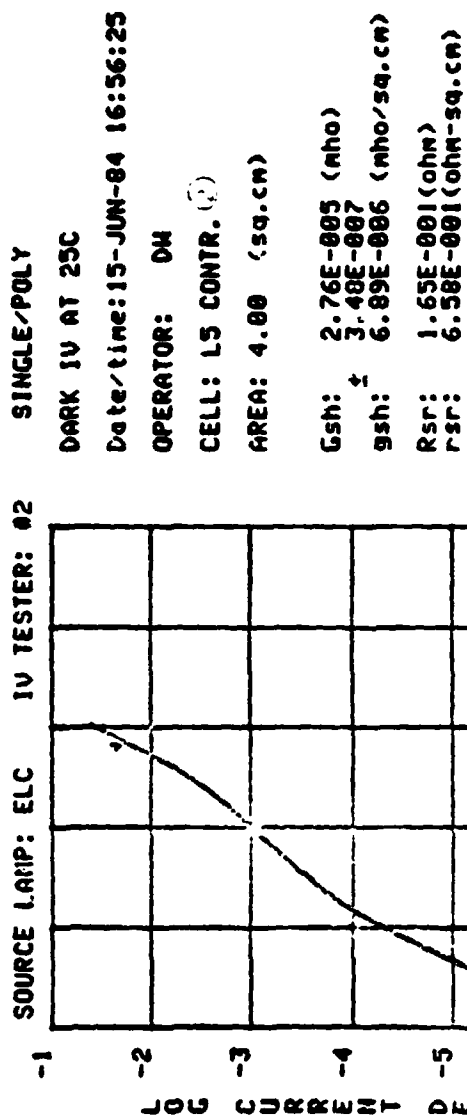


Fig. 18b.

The extremely low V_{OC} on L5A #7 was due to insufficient surface concentration which also affected the sheet rho uniformity across the surface causing leakage as revealed by reverse dark I-V measurement.

The poor result with caustic polished Cz wafers suggested the use of chem-mechanically polished FZ of 0.3 ohm-cm p-type wafers as a baseline experiment. The material had been well characterized by conventional thermal diffusion that yielded efficiency of 16% at AM1.5 with simple spin-on A/R coating for cells of 25 cm² total area (Fig. 18).

Material from this batch was sent for ion implantation with 31p+ at 5 keV of dosage 1x10¹⁵, 2.5x10¹⁵ and 5x10¹⁵ atoms/cm², respectively. Laser energy varied from 0.90 to 1.30 J/cm², with overlap from 20% to 70%. Pulse duration time was extended from 6 ns to 50 ns (double pulse shape). The reason for overlap was to compensate beam non-uniformity. As beam quality was progressively improving, the overlap factor was decreasing proportionally. Results are summarized in Table 6.

Table 6. Results of laser annealing on chem-mech polished wafers 5 keV ion implanted with 1x10¹⁵ and 2.5x10¹⁵ atoms/cm² dosage, respectively.

Cell ID (FZ)	5 keV Ion Dosage, 10 ¹⁵ atom/cm ²	Laser Energy Density, J/cm ²	Over-lap, %	V_{OC} , V	J_{SC} , mA/cm ²	FF, %	Eff, %	Sheet Rho, ohm/sq
B9-1								
#1	2.5	1.30	70	0.554	18.23	75.00	7.58	40-45
#2	2.5	1.30	70	0.552	18.22	75.70	7.62	40-45
#3	2.5	1.30	70	0.555	16.61	73.00	6.79	40-45
#4	2.5	1.30	70	0.544	17.74	67.22	6.48	40-45
#5	2.5	1.30	70	0.543	18.33	71.72	7.14	40-45
B9-2								
#1	2.5	0.90	70	0.579	21.36	48.13	5.96	50-55
#2	2.5	0.90	70	0.583	21.13	55.92	6.89	50-55
#3	2.5	0.90	70	0.531	21.17	60.21	6.77	50-55
#4	2.5	0.90	70	0.593	21.12	67.20	8.42	50-55
B10-1								
#1	1	0.90	30	0.534	21.74	70.24	7.70	65-74
#2	1	0.90	30	0.548	22.64	70.74	8.78	65-74
#3	1	0.90	30	0.553	22.58	72.17	9.01	65-74
#4	1	0.90	30	0.552	22.36	68.97	8.51	65-74
B10-2								
#1	1	1.25	20	0.569	21.77	70.68	8.75	60-75
#2	1	1.25	20	0.577	21.95	71.32	9.03	60-75
#3	1	1.25	20	0.572	21.96	70.67	8.87	60-75
#4	1	1.25	20	0.573	21.59	72.12	8.92	60-75

In experiment B9-1 where laser energy density was as high as 1.3 J/cm² with 70% overlap, both current density and V_{OC} were very low. The latter was probably due to excessive surface damage,

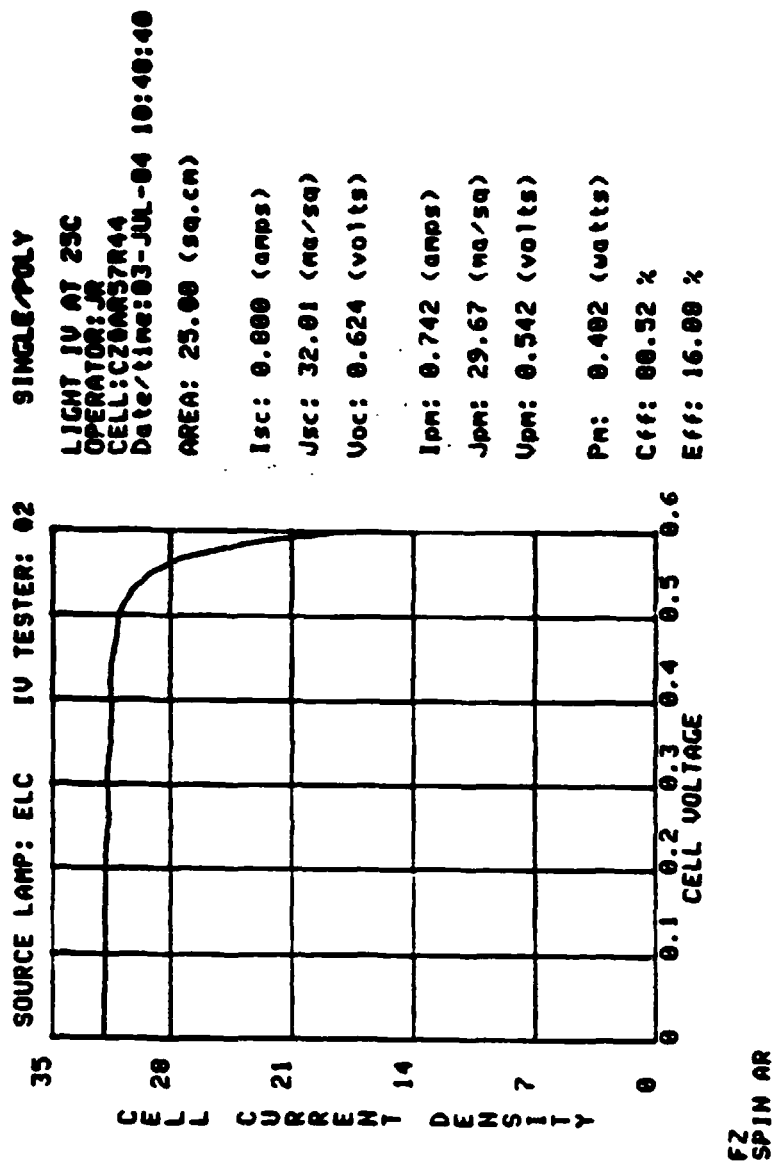


Fig. 19. Baseline Material Characterization on Fz Wafers by Thermal (POCl_3) Diffusion. Spin-On A/R Coating.

especially at the center of overlap (Fig. 20). The former was due to the deep junction characteristic that limited the J_{sc} to less than 18.5 mA/cm^2 . However, the deep junction helped to improve the fill factor on average.

All cells annealed at 0.9 J/cm^2 (B9-2) had high leakage current and low shunt resistance that affected the fill factor.

The general trend of the above experiments suggested that reduction in overlap % (to the limit where beam uniformity fails to anneal the whole area), the better the cell performance. There was not much effect due to dosage difference from 1×10^{15} to 2.5×10^{15} atoms/cm². Also, examination of literature data suggested that a minimum of overlap is required to obtain the highest efficiencies. As a result, the start-up and use of a higher power, larger beam size (spot size $\geq 0.7 \text{ cm}^2$) laser, at MSNW was initiated. Two initial experiments were conducted. Results obtained were encouraging. (See Table 7.)

Table 7. First experimental result with the larger laser, at density 1.4 and 1.6 J/cm² respectively.

Cell ID (FZ)	5 keV Dosage, $\times 10^{15}$	Energy Density, J/cm^2	Over- lap, %	Pulse Duration ns	V_{oc} , V	J_{sc} , mA/cm^2	FF, %	Eff, %	Rho, ohm/sq
B-11									
#1	2.5	1.3	20	80	0.569	21.47	67.95	8.31	46-65
#2	2.5	1.3	20	80	0.581	21.06	62.15	7.60	46-65
#4	2.5	1.3	20	80	0.587	21.53	74.18	9.37	46-65
#5	2.5	1.3	20	80	0.583	21.36	67.56	8.41	46-65
B-12-2.5E									
#1	2.5	1.6	8	80-90	0.593	20.14	78.50	9.38	40-53
#2	2.5	1.6	8	80-90	0.580	20.02	71.17	8.26	40-53
B-12-5E									
#1	5	1.6	8	80-90	0.593	20.40	70.62	8.55	26-32
#2	5	1.6	8	80-90	0.593	20.54	73.89	9.01	26-32

Although the junctions formed here were deeper than previous experiments, as indicated by the lower sheet resistivities, both the V_{oc} and J_{sc} were comparatively higher on average. A fill factor as high as 78.5% was also obtained (B-12-2.5E #1). Results suggested the advantage of a more powerful laser of larger beam size with more output uniformity that allowed less total overlap.

Two more experiments with different combinations of energy and % of overlap were then immediately conducted: 0.95 J/cm^2 with 9% overlap and 1.1 J/cm^2 with 7% overlap, respectively. Results are summarized in Table 8.

ORIGINAL PAGE IS
OF POOR QUALITY

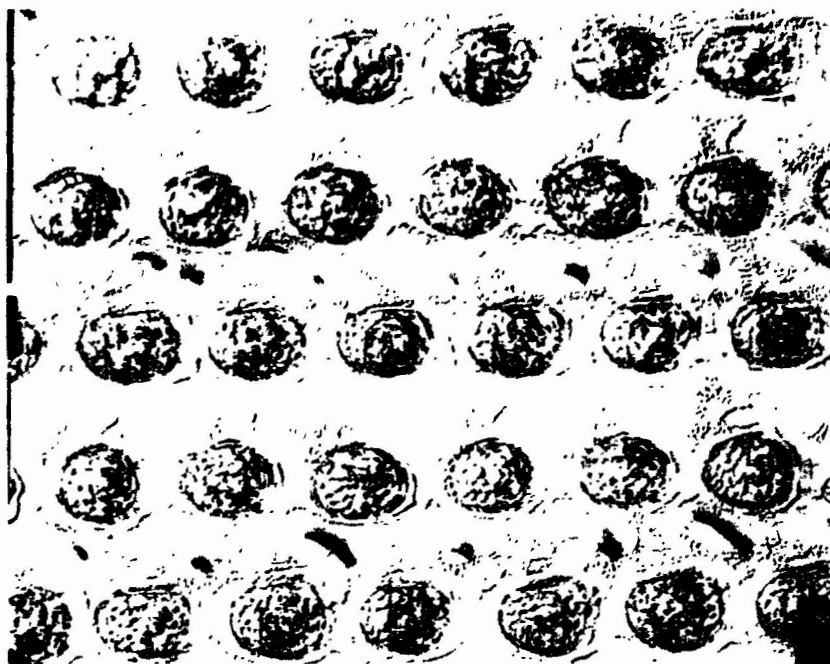


Fig. 20. Laser Annealing on 5 KeV, 2.5×10^{15} atom/cm² Ion Implanted Surfaces at 1.3 J/cm², With 70% Overlap Pulse Duration Estimated 6ns (B-9).

Table 8. Results of annealing by the larger laser with lower energy density and overlap %.

Cell ID (FZ)	5 keV Dosage, $\times 10^{15}$	Energy Density, J/cm^2	Over-lap, %	V_{OC} , V	J_{SC} , mA/cm^2	FF, %	Eff, %	Sheet Rho, ohm/sq
B-13								
#1	5	0.95	9	0.495	21.30	49.93	5.26	>100
#2	5	0.95	9	0.531	20.80	52.29	5.78	>100
#4	5	0.95	9	0.425	21.81	41.87	3.88	>100
#5	5	0.95	9	0.554	21.54	52.80	6.30	>100
B-14								
#1	5	1.10	7	0.531	22.71	58.78	7.09	68-80
#2	5	1.10	7	0.533	22.99	58.80	7.20	68-80
#3	5	1.10	7	0.512	22.69	53.58	6.23	68-80
#4	5	1.10	7	0.477	20.37	44.59	4.33	68-80

All cells showed high series resistance and high shunt conductivity due to shallow junction as well as insufficient overlap. The other factor considered to be contributing to the low V_{OC} was the presence of ion implantation damage that was not removed at such low energy densities.

In order to isolate the effects of ion implantation such as nonuniformity and lattice damage, a special experiment was conducted in which Cz polished wafers (0.7 ohm-cm) were subjected to N^+ deposition at 830°C using POCl_3 as the dopant source. Sheet rho after the phosphorus glass was removed was about 200 ohms/sq . A wafer with the phosphorus glass still remaining was then laser annealed at $1.25 \text{ J}/\text{cm}^2$ with 10% overlap. Sheet resistivity after annealing was as low as 15 ohms/sq . Cells were fabricated only after etching back to 60 ohms/sq . Highest efficiency was 10% without A/R. In parallel to the laser annealing, control cells were made from similar wafers that had been subjected to thermal diffusion. As shown in Table 9, results of the laser annealed and that of the thermally diffused were quite alike.

Table 9. Laser annealing for wafer with thermal N+ deposition. Control cells were thermally diffused. All cells without A/R.

Cell ID (Cz)	N+ Deposition Temp (°C)	Laser Energy Density	Over- lap, %	V _{oc} , V	J _{sc} , mA/cm ²	FF, %	Eff, %	Sheet Rho on Cells
B-15								
#1	830	1.25	10	0.588	22.15	76.89	10.01	60-65
#2	830	1.25	10	0.587	21.82	76.36	9.78	60-65
#3	830	1.25	10	0.568	21.04	76.37	9.12	60-65
#4	830	1.25	10	0.588	21.82	76.49	9.81	60-65
Control								
Special								
B-15								
#1	830	Thermal Diffuse	--	0.586	21.64	74.02	9.38	60-70
#2	830	--	--	0.593	22.54	75.97	10.14	60-70
#3	830	--	--	0.592	22.37	77.58	10.28	60-70
#4	830	--	--	0.592	22.00	77.93	10.16	60-70

In fact, the dark and light I-V curves of the typical cell in each group were almost identical (Fig. 21).

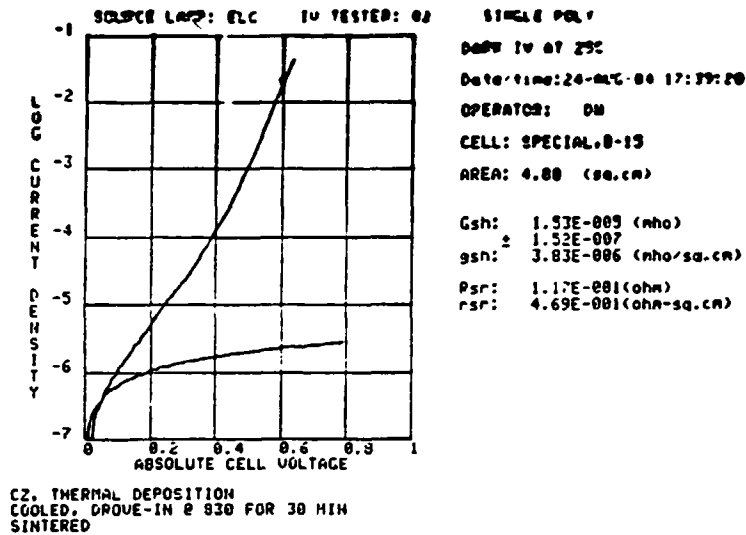
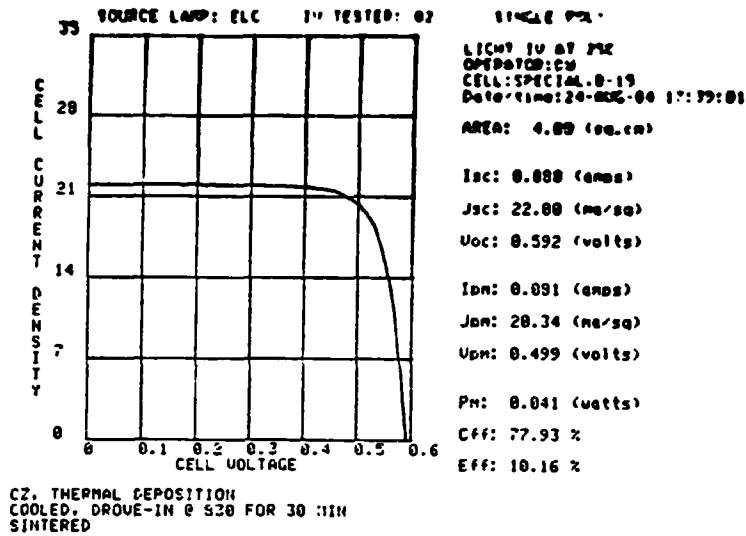


Fig. 2la. Light and Dark I-V Curves for Typical Cells From Thermal N+ Deposition and Diffusion.

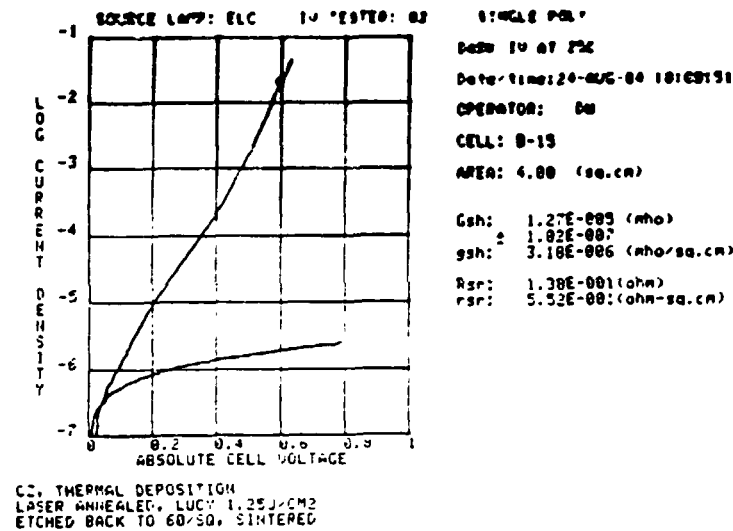
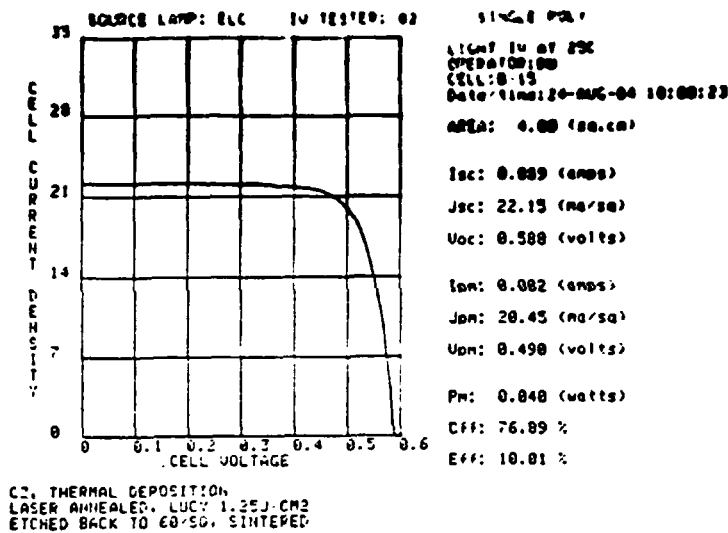


Fig. 21b. Light and Dark I-V Curves for Typical Cells From Thermal N+ deposition and Laser Driven In at 1.25 J/cm², 10% Overlap.

4.0 DISCUSSION OF EXPERIMENTAL RESULTS

The laser annealing experiment started with spin-on liquid dopant for convenience and for economic reasons. Surface conditions included sodium hydroxide texture and polish. Due to the increase in absorption, spin-on dopant caused more surface damage than expected, especially at the overlap area where melting was more severe.

Damage on a textured surface with spin-on coating was even greater. Because of the pyramid surface structure, 0.4 J/cm^2 was found sufficient to cause melting. The degree of melting at different energy densities can be visualized from Figure 16. At 1.2 J/cm^2 , the surface was almost recrystallized, losing most of the texturing property. Spin-on dopant on either polished or textured wafers for laser annealing requires more experimentation.

Laser annealing of phosphorus ion implanted wafers was also extensively investigated. Results were far from ideal. Two of the most important factors were the beam uniformity and high implantation energy.

Model calculations of the depth and duration of pulsed excimer laser melting as a function of energy density predicted the threshold of 0.9 J/cm^2 for surface melting, 1.5 J/cm^2 to a depth of $0.166 \text{ }\mu\text{m}$ and 1.75 J/cm^2 to a depth of $0.266 \text{ }\mu\text{m}$ (Young, 1982). The SIMS depth profile for a 5 keV phosphorus ion implant sample (Fig. 21) suggested the ion channeling distance was almost $0.16 \text{ }\mu\text{m}$. Both the calculated melt depth and ion channeling distance suggested that the threshold energy required to completely remove lattice damage caused by a 5 keV implant would be at least 1.5 J/cm^2 (90 ns pulse). Experiment B-9-1 was conducted at 1.3 J/cm^2 with the small laser. However, the 70% overlap caused severe surface damage (Fig. 20) that limited the V_{oc} to less than 0.56 V. Current recombination at the damaged areas are clearly shown by the laser scan photo (Fig. 23).

By using the larger laser (5 J max power) with greater uniformity and area coverage, less overlapping was necessary. Maximum cell efficiency of 9.4% without A/R (13.7 with A/R) was obtained with 1.6 J/cm^2 energy density. V_{oc} on average was the highest among all experiments. Results were in agreement with the calculated melt depth and lattice damage by ion implant described above.

The effect of unremoved lattice damage was further demonstrated indirectly by laser annealing a thermal N^+ deposition wafer. 10% maximum cell efficiency was the result for a Cz wafer. Had the phosphorus glass been thinner before annealing, higher cell efficiencies would be obtained. The V_{oc} was still comparatively lower (5-8 mV) than thermally diffused cells. This is believed to be due to recombination at the overlap boundaries.

PROCESSED DATA

CHARLES EVANS & ASSOCIATES

7/18/84

DEPTH PROFILE

8) P) S1 5KeV 2.5e15

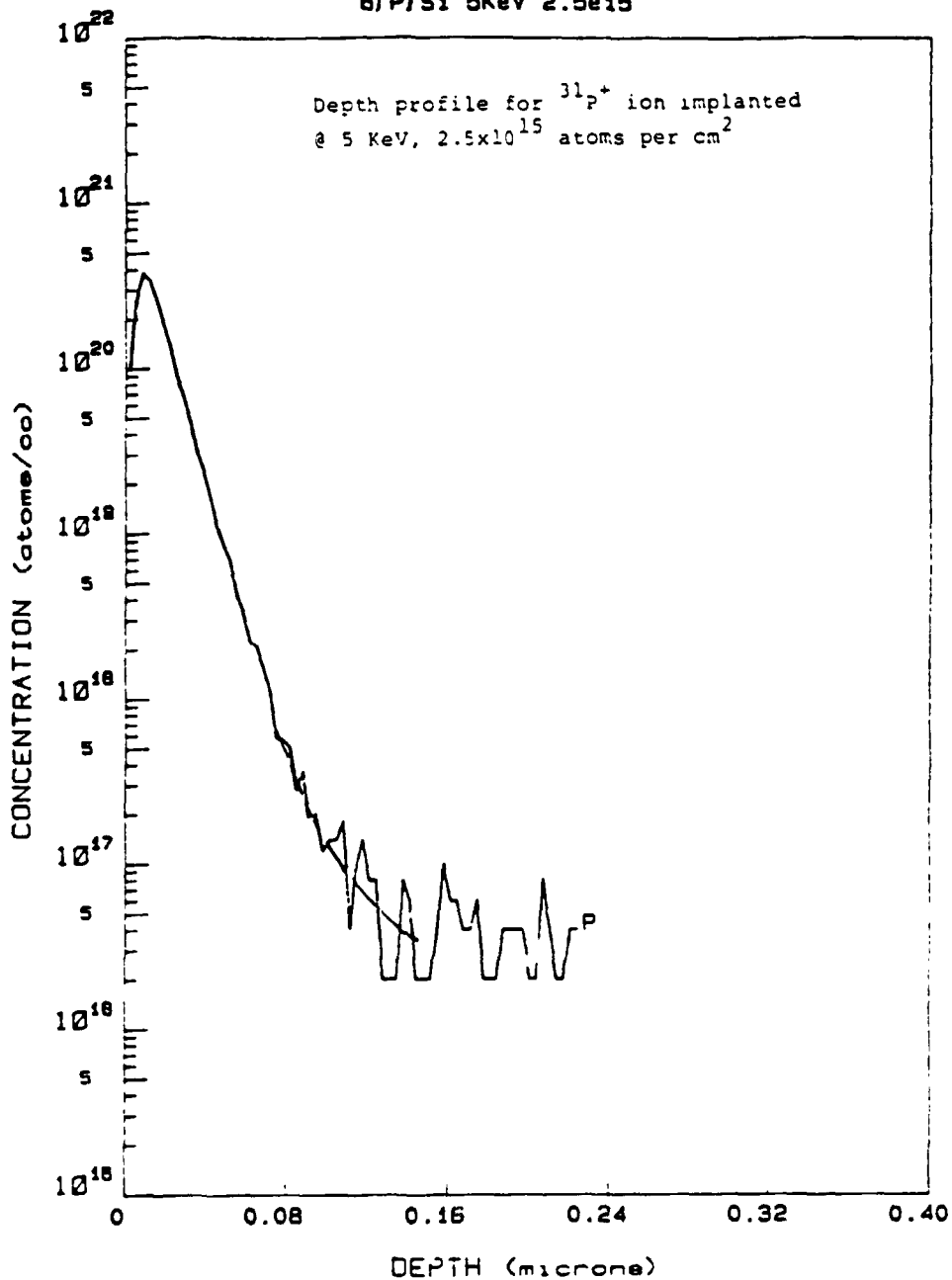


Fig. 22. SIMS Depth Profile for $^{31}\text{P}^+$ Ion Implanted at 5 keV, 2.5×10^{15} Atom per cm^2 . Substrate Resistivity ~ 0.3 ohms-cm Boron Doped.

ORIGINAL DOCUMENT
OF POOR QUALITY

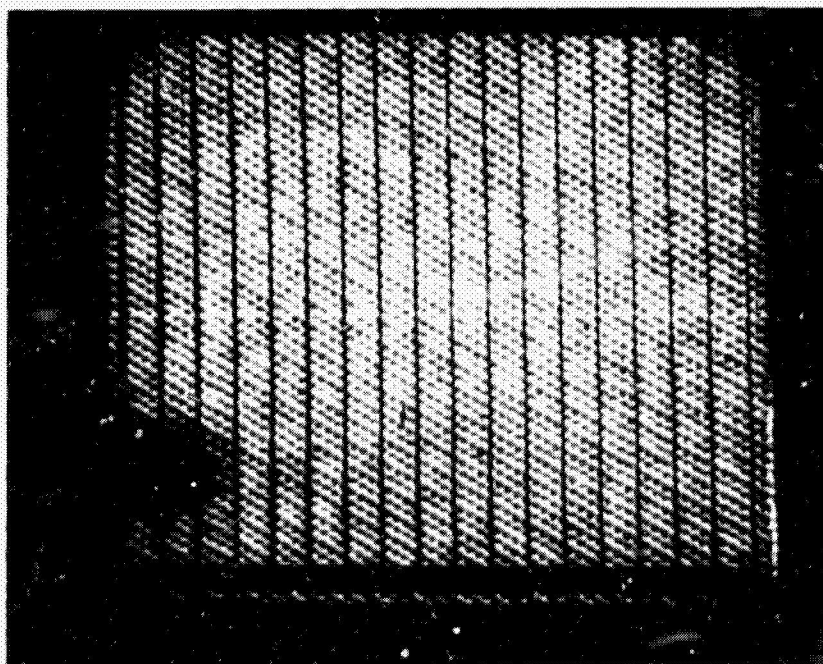


Fig. 23. Laser Scanning at the Highly Damaged Surface That Was Laser Annealed at 1.3 J/cm^2 , 70% Overlap Factor (B9-#4). Heavy Recombination at the Center of Overlapped Area is Clearly Revealed.

5.0 TARGET PROCESS SELECTION REPORT

5.1 PROCESS SELECTION

A description of the selected baseline and excimer laser process sequence follows.

5.1.1 Baseline Prices

The baseline process is essentially the same as the JPL state-of-the-art process. The only difference being the absence of a back surface formation step and the use of plasma etching. This operation has been amenable to higher throughput than the individualized laser scribing technique. A flow diagram of the baseline process is shown in Figure 24. The process utilizes Czochralski grown p-type (Boron doped) (1-0-0) wafers of 5.2" diameter and nominal resistivity of 0.3 ohm-cm. The nominal wafer thickness is 400 μ m.

A sodium hydroxide (NaOH) etch is used to remove the damaged surface layer (sawing damage). This etching step removes 50-75 μ m of the surface layer. The etched surface is then subjected to an anisotropic texturing etch utilizing dilute (2%) NaOH solution. Dilute NaOH preferentially etches (100) crystallographic planes more rapidly than the (111) plane leading to a surface finish that consists of tetrahedrons projecting upwards from the silicon surface. These tetrahedrons act as very efficient light traps. The textured surface is then cleaned in a dilute H₂SO₄ acid solution and is rinsed in deionized water and dried.

The textured surface is then subjected to a diffusion step to form the p-n junction. Phosphorous oxychloride is used in a gas diffusion tube to deposit a phosphorus rich n-layer on the p-type wafer. The phosphorus is then driven into the silicon to form the p-n junction. This diffusion/drive-in process is carried out at a high temperature (850°C). The resulting junction is typically 0.3 μ m deep. The sheet resistance of the diffused surface region ranges between 35-40 ohms per square. To remove any shunting path between the front and back surface of the cell, the edges of the diffused cell are etched in a plasma etcher using a fluorocarbon-oxygen mixture. Ohmic contacts to the cell are made by screen printing a grid pattern of silver paste on the front and back surface of the cell. The contacts are dried and then sintered in a conveyor fed infrared furnace. This processing sequence typically yields cells with the following parameters

$$J_{sc} = 30 \text{ mA/cm}^2; V_{oc} = 585 \text{ mV}; ff = 0.74; EFF = 13.0\%$$

The fabricated cells are then assembled and laminated into modules using the JPL state-of-the-art process.

PRECEDING PAGE BLANK NOT FILMED

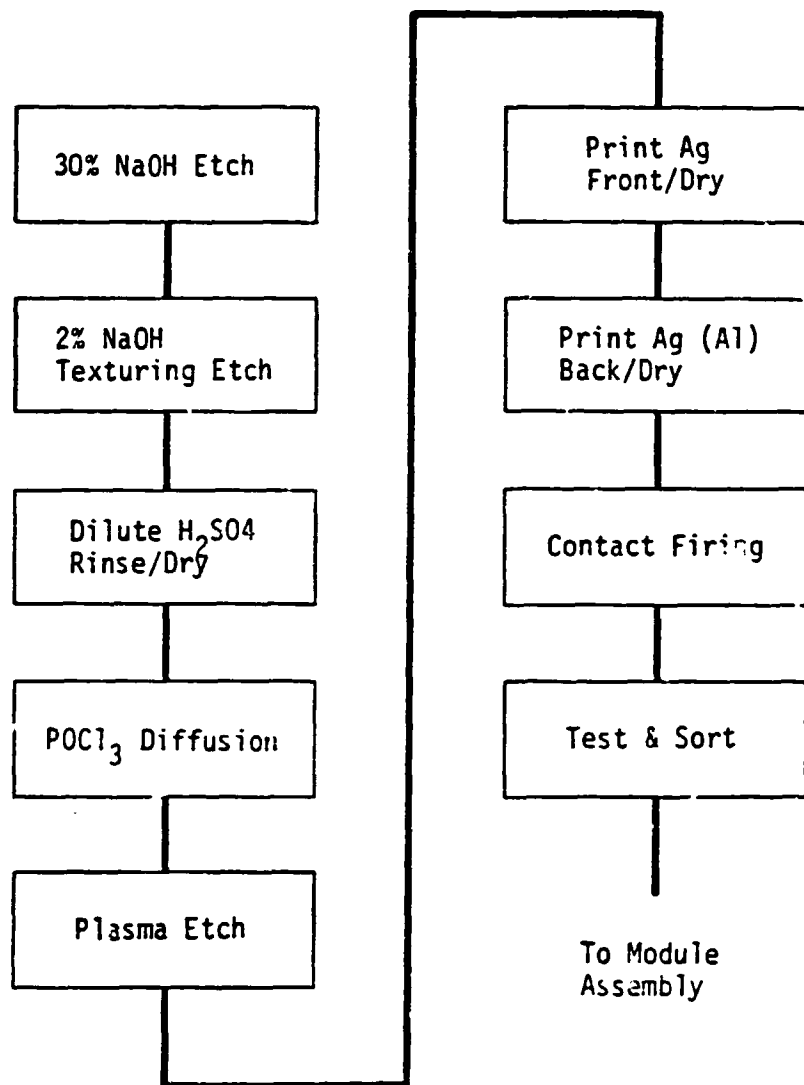


Fig. 24. Baseline Process. 5.2" Diameter, P Type (Boron Doped) 0.3 ohm-cm Cz Silicon.

5.1.2 Description of the Preliminary Laser Process

A schematic of the selected laser processing sequence for the fabrication of solar cells is shown in Figure 25. Phosphorus doped n type Czochralski grown silicon (100) wafers of 5.2" diameter and nominal resistivity of 0.3 ohm-cm will be used (range 0.1 - 0.3 ohm-cm). The nominal wafer thickness will be 400 μm . A sodium hydroxide etch will be used to etch the wafer surface to remove the damaged surface layer (50-75 μm). The etched surface will be subjected to an anisotropic etch (2% NaOH) to texture it. The textured surface will then be cleaned in dilute H_2SO_4 solution. The surface is rinsed in deionized water and dried.

The textured surface is then subjected to an ion implantation process as a first step towards a p-n junction formation. The front surface of the cell will be implanted with Boron (^{11}B) at an energy of 5 keV and to a dose of 6×10^{15} atoms/ cm^2 . A Spire Inc. continuous ion implanter is an example of the equipment to carry out this implant. After ion implantation, the samples will be cleaned with acetone, methanol, $\text{H}_2\text{O}_2:\text{H}_2\text{SO}_4(1:1)$, $\text{HNO}_3:\text{H}_2\text{SO}_4(1:1)$ and $\text{HF}:\text{H}_2\text{O}(1:10)$ to remove any organic and metallic contaminants prior to laser annealing.

The annealing of the boron implanted region would be carried out using a high power excimer laser such as the XMR XL-150. This laser has a wavelength of 308 nm when operated using XeCl gas. A beam energy density of 1.2 J/ cm^2 will be utilized at the work surface. The laser will be pulsed at 500 Hz. The pulse width of the laser is 50-80 nsec. A beam width of 0.35 x 0.35 cm^2 will be utilized. The annealing will be done in air. One pulse per 0.125 cm^2 area will be required. Overlap is assumed to be minimal, below 5%. The annealing process will require about 1025 laser pulses to cover the surface. The time to carry out the annealing will be about 3 seconds including wafer transport time. The laser is expected to melt the silicon surface to a depth of approximately 0.3 - 0.5 μm and result in a junction depth in the 0.15 - 0.2 μm range. The laser annealed samples will be cleaned in a $\text{HF}:\text{H}_2\text{O}(1:10)$ solution, rinsed with deionized water and dried. The back surface of the cell will be metallized with an 2000 \AA thick layer of nickel phosphide.

The front surface of the solar cell will have an intentionally grown passivating thin oxide layer to minimize the carrier recombination along the cell top surface. The oxide has to be thin (~15-20 \AA) so that carriers can tunnel through it and to be efficiently collected by the front grid pattern. This technique has yielded cells with high open circuit voltage and consequently higher efficiency. A laser assisted process will be used to grow this thin oxide. The oxide growth will be carried out in a $\text{N}_2\text{O}/\text{SiH}_4$ ambient at a pressure of 6 torr and at a substrate temperature of $<300^\circ\text{C}$. The laser used for this process will be an excimer ArF laser (193 nm). Deposition rates in the 600 $\text{\AA}/\text{min}$ to 800 $\text{\AA}/\text{min}$ have been observed using these deposition

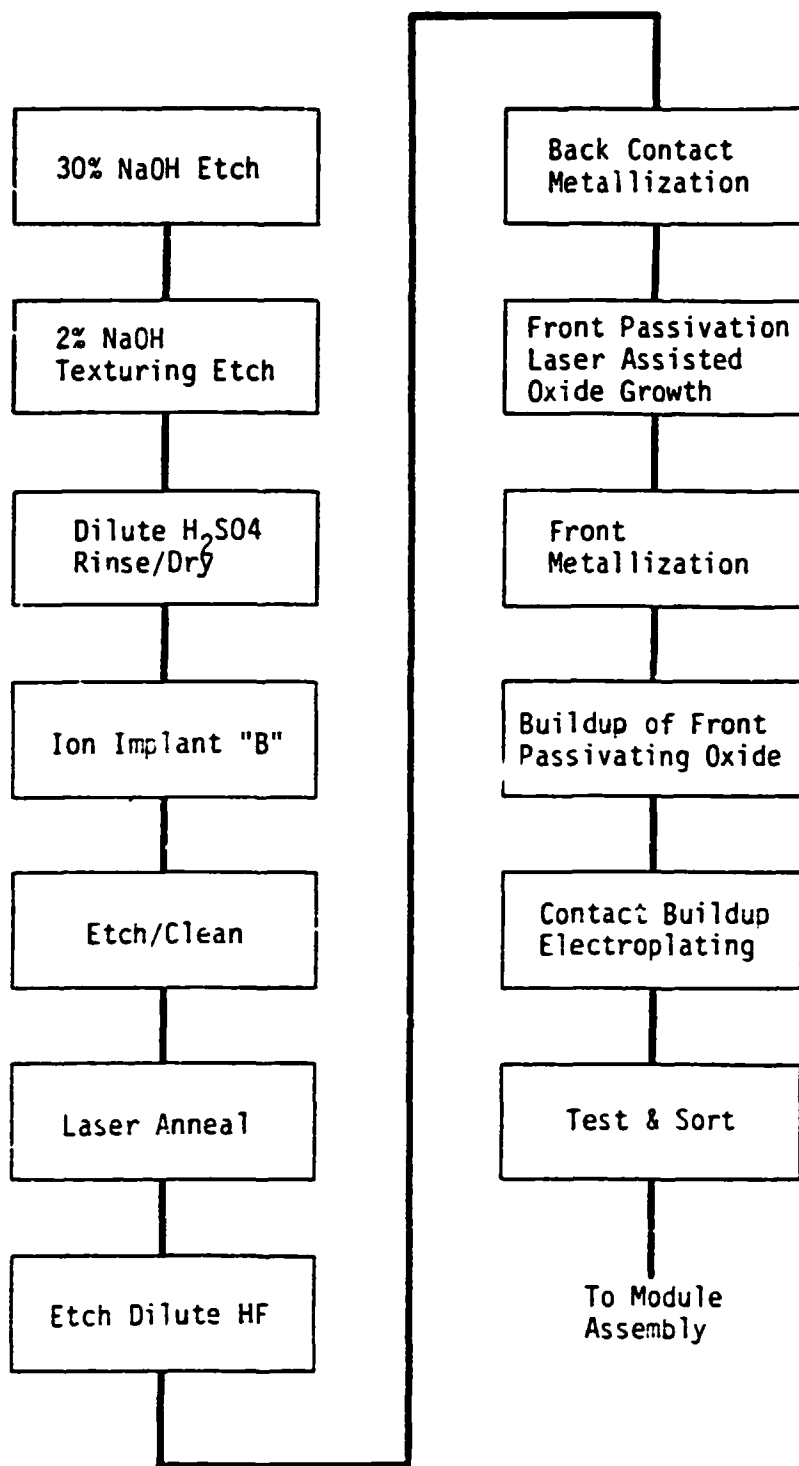


Fig. 25. Preliminary Laser Process. 5.2" Diameter, N Type (Phosphorus Doped) 0.3 ohm-cm Cz Silicon.

conditions. Deposition rates in this range are appropriate for achieving good control of the oxide thickness in the desired range (15-20 Å). The properties of these laser grown oxides have been shown to be comparable to oxides grown using plasma enhanced and mercury photosensitized chemical vapor deposition.

The passivated cells will be coated with gridlines on the front surface using laser assisted pattern writing on semiconductors. This deposition will be carried out to a thickness of 2000Å of aluminum so that the buildup of the gridline thickness using electroplating is possible. The laser beam will be optically configured to write thin narrow lines. The laser energy density has to be low enough so as not to damage the p-n junction formed during the laser anneal but still has to be high enough to provide metal deposition rates that are meaningful for scale-up of this process (i.e. a 1000 Å/min rate at the minimum).

After gridline deposition, the cell front surface will be subjected to a second oxide growth step to provide passivation of the front surface in between the gridlines. Oxide growth will be carried out in a fashion similar to the one discussed above. However, the oxide will be grown to a greater thickness (=100Å). This thickness of the intergrid oxide has been demonstrated to provide good passivation of the front surface leading to high open circuit voltage. Once the front surface passivation has been carried out, the thickness of the gridlines and the back contact will be increased to 7 µm by utilizing electrochemical techniques to plate nickel phosphide on the gridlines to increase their electrical conductivity and thereby increase their ability efficiently to extract the photogenerated current. The cells then are encapsulated using the JPL baseline process.

5.2 ECONOMIC ANALYSIS

5.2.1 Approach

Development of a simplified methodology which permits increased flexibility in performing price estimation of individual process elements was described by (Aster, 1980) with the publication of the Improved Price Estimation Guidelines (IPEG). The equation and coefficients which were generated at that time provided closer agreement with SAMIS results than the earlier versions. An IPEG calculation for each process step has been prepared. Changes from the baseline process were substituted into the baseline and the module final cost recalculated. These estimates employ the recently revised IPEG coefficients listed in Table 9. The baseline sequence is called the JPL Sample Process.

In order to perform an estimate, the cost elements required for the IPEG calculation have been individually developed for each process step. The following sections discuss the assumptions associated with the required process equipment and its installation, operation and maintenance scenarios. Based on throughput and use factor estimates, the required labor,

materials, and utilities to maintain an annual production capacity of 5 MW were developed for each of the proposed processes.

5.2.2 Results

Tables 10 and 11 provide a direct comparison of costs for the baseline process, and the proposed laser process sequence. The calculated baseline cost estimate is \$2.98, using an assumed cell efficiency of 13%. Table B indicates a cumulative potential cost reduction of \$0.66 per peak watt if the proposed laser methods are fully implemented.

When comparing costs to the JPL Sample Process sequence, it is necessary to consider the resultant cell output and module efficiency (taken as 9.6% for the sample sequence), and the effect or expected improved cell efficiency and larger wafer size on the number of units processed annually to achieve required production volumes. If the predicted improved efficiency of 17% is achieved, and the 5.2 inch wafers can be processed at the predicted yields, then the module efficiency at the stated conditions (NOC) will approach 11.7%. This will reduce the costs of subsequent process steps by virtue of fabrication of 21% fewer modules/year. For example, if a module geometry of 0.6 x 1.2 m is chosen as the design point, a total of 90,422 modules are required to be equivalent to five megawatt for a 9.6% efficiency (at NOC) module design. However, using 17% efficient cells (which yield a module efficiency of approximately 11.7%) only 74,192 modules were required. Immediately obvious benefits from this reduced build-requirement are proportional reductions in the labor content of all process steps and, for those steps which are assembly or test sequences, the entire cost will be reduced substantially (e.g. cell layup, material preparation, layup trim seal test and package module). Attendant to these reductions are similar reductions in material usage. For example, the total area of glass superstrate is reduced by 11,685 m². At a 1983 quantity price of \$9.92/m² quoted by glass manufacturers for 1/8" tempered low-iron AR treated glass, a cost reduction can be calculated (using the IPEG materials coefficient of 1.17) as:

$$\$/W_{pk} = \frac{1.17 \times \$9.92 \text{ m}^2 \times 11,685 \text{ m}^2}{5 \times 10^6} = \$0.027$$

Similar reductions in other module direct materials requirements such as encapsulant, substrates and frames have been calculated.

Additionally, process yields were estimated for the laser process sequence which result in a net cumulative process sequence yield equivalent to the JPL sample process. Implementation of the proposed laser process will employ relatively "cold" methods including the use of a handling pallet which positions and supports the wafers through the majority of the cell manufacturing steps. Thus, the incidence of yield losses due to mechanical breakage, will be significantly reduced.

TABLE 10

COST SUMMARY - JPL SAMPLE SEQUENCE

PROCESS STEP	EQUIP*	IPEG FT2	COST DLAB	ELEMENTS MATLS	UTIL	EST \$/WPK	YIELD	REMARKS
"WETLINE" - 30% NaOH - 2% Text Dil H2SO4 Rinse/Dry	\$180,000	990	48,200	92,600	7,500	.0698	0.989	Assumes automated line
POCl ₃ DIFFUSE								Assume JPL Sample Seq.
				JPL JUNCTION DIFFUSION PROCESS		0.048	0.988	
PLASMA ETCH	180,000	300	27,000	92,800	30,000	0.180	0.980	
COMBINED PRINT/ DRY/FIRE Ag FRONT AND BACK CONTACTS								Assume JPL Steps Include Firing
				JPL SAMPLE PROCESS SEQUENCE		0.180	0.980	
JPL SORT AND MODCO				JPL TEST/SORT & MODCO SEQUENCE USED		0.590	0.935	JPL Sample Sequence
SI SUBSTRATE				VALUE ADJUSTED FROM \$1.91 FOR 13% CELL AND 127.5 CM ²		2.050	1.000	Baseline Process @ 13%
				TOTAL MODULE FINAL COST		12.980	0.886	

TABLE 11

COST SUMMARY - PROPOSED LASER PROCESS

PROCESS STEP	IPEG COST ELEMENTS			EST	YIELD	REMARKS
	EQUIP	FT2	DLAB	MATLS	UTIL	\$/WPK
WETLINE	\$180,000	990	\$48,200	\$ 96,600	\$7,500	0.07
ION IMPLANT	330,000	50	35,900	35,980	1,326	0.03
H2O2:H2SO4 ETCH	74,000	240	24,100	48,000	2,500	0.03
LASER ANNEAL	302,160	140	16,800	7,200	2,900	0.02
10:1 HF CLEAN	30,000	200	19,280	9,000	1,000	0.02
BACK CONTACT EVAP. METAL	600,000	250	28,080	30,000	8,000	0.04
LASER PASSIVATE FRONT OXIDE	81,500	78	17,974	32,271	422	0.02
FRONT CONTACT LASER WRITE	203,000	138	32,360	94,540	1,097	0.04
CONTACTS ELECTROPLATE	29,500	80	55,680	500	2,065	0.03
JPL CELL SORT AND MODCO	-	-	-	-	-	0.45
Si SUBSTRATE	-	-	-	-	-	1.58
TOTAL MODULE COST					2.32	0.886

JPL has documented this sample process sequence with a complete set of SAMICS Format A forms and performed a computer SAMIS run to calculate these costs. As a result of the detailed computer run, IPEG coefficients have been calculated. These are:

$C_1 = 0.59$	for annual equipment cost (EQPT)
$C_2 = 136$	for annual factory area cost (FT ²)
$C_3 = 2.02$	for annual direct labor cost (DLAB)
$C_4 = 1.17$	for annual material cost (MATS)
$C_5 = 1.17$	for annual utilities cost (UTIL)

Fig. 25. IPEG Coefficients for JPL Sample Process Sequence.

5.2.2.1 Discussion of Cost Elements of Excimer Laser Applications

(a) Equipment Costs

The initial cost of present commercial excimer lasers ranges from \$10-15K for lower power devices (\leq watt) to \$40-50K for the highest power devices (20-30 watts). The higher power devices that are anticipated (50-200 watts) will range in cost from \$100-400. Thus the normalized cost of near term excimer laser equipment is approximately \$2500/watt in the 10 to 200 watt range. The wavelengths available are 193, 248, 308, and 351 nm.

(b) Laser Operating Costs

There are three principal cost elements associated with excimer lasers; the consumption of excimer laser gas, the use of electricity and other utilities, and scheduled maintenance to replace or repair short lifetime components. Typical costs per watt-hour of excimer laser output are \$0.05 (ArF or XeCl) to \$5.0 (KrF) for laser gas, \$0.02 to \$0.05 for electricity, and \$0.2 to \$2.0 for scheduled maintenance. Reduction of gas consumption and maintenance costs is one of the critical development steps required for the successful application of excimer laser technology to solar cell fabrication.

Recent promising developments in the United Kingdom in the area of excimer gas on-line reprocessing have demonstrated significant reductions in gas replenishment frequency, especially for ArF. A reduction of 20:1 in gas consumption is assumed in this cost estimate.

In the area of maintenance, the principle driving costs involve frequent refurbishment and replacement of internal parts affected by the excimer gas and the high switching pulse loads on the thyatron. In particular, efficient laser operation requires complete teardown of the laser optical system about every 1×10^8 shots. This is approximately once a week for the proposed ArF laser.

An advantage of the XMR XeCl high power laser is that it does not use thyatrons for pulse switching so the maintenance cost is much reduced from the ArF laser as can be seen in the detailed paragraphs.

5.2.3 IPEG Analysis of Specific Laser Processes

(a) General

Each IPEG cost elements is discussed below on a process-by-process basis. The following assumptions, consistent with IPEG procedures, were used throughout the analysis:

1. Equipment Capital Costs (EQPT) include installation and first year's major component spares, reduced by salvage and removal value.
2. Equipment has a 7 year life and uses straightline depreciation.
3. Facility Area (FT²) includes equipment footprint area and required working space for normal operation.
4. Direct Labor (DLAB) includes, as applicable, factory manufacturing and maintenance personnel at the following hourly direct rates (excluding fringes):

Technician/Operator	- \$ 6
Senior Processor	- \$ 8
Maintenance	- \$10
Process Engineer	- \$12

5. Direct Material Costs (MATLS) are based on best estimates from actual laser operating experience and include scheduled maintenance materials.
6. Utility Cost (UTIL) is based on \$0.75/KWHR rate. KWHR demand is calculated on basis of operation for estimated equipment availability factor of 0.85.

(b) Laser Annealing

1. EQPT - Process rates require one XeCl laser system operating at 55% capacity thus, a spare system would not be required. Wafer transportation is assumed to be cassette-to-cassette.

1 XC-150 XeCl laser	- 232,000
1 precision N/C table	- 10,000
1 microprocessor	- 3,000
1 gas reproprocessor	- 35,000
1 K-bottle/manifold bank	- 2,000
1 wafer transport system	- 2,000
Installation - 2 man mos	- 8,160
Less salvage @ 10,000	- <u>10,000</u>
EQPT TOTAL	= 302,160

2. FT² - Approximate area for laser and associated equipment is:

$$FT^2 \text{ total} = 14' \times 10' = 140 FT^2$$

3. DLAB - The laser anneal facility is operated for 2300 hours by one technician. All scheduled/routine maintenance is performed by skilled electro-mechanical maintenance technicians:

$$\text{Operation } 2300/\text{yr @ } \$6 = \$13,800$$

Maintenance 300/yr @ \$10 = \$ 3,000
DLAB TOTAL = \$16,800

4. **MATLS** - Principal direct costs are the replacement parts for the laser systems. Gas consumption assumes that the gas reprocessor can achieve a 16:1 extension of gas life.

o Gas consumption, annual = \$8,680
53 hours/fill; 2300 hours/year; 200 \$/fill
MATLS TOTAL = \$8,680

5. **UTIL** - Estimated electric demand for the laser anneal facility includes cell transport and location at 0.5 Kw; control electronics at 0.2 Kw; and laser power requirement of 15.8 Kw.

Annual KWHR = \$37,950
Rate = .075
UTIL TOTAL = 2,900

(c) **Laser Front Contact Metallization**

1. **EQPT** - Based on rates described, two ArF lasers operating one microprocessor, one gas reprocessor, reactant gas pumping and reclaim system, and wafer transport and locating equipment for the laser writing are required:

2 EXC-2 ArF lasers @ 27,000	= \$ 54,000
1 gas reprocessor @ 10,000	= 10,000
2 N/C tables @ 10,000	= 20,000
1 microprocessor @ 3,000	= 3,000
1/2 K-bottle bank @ 1,000	= 1,000
(shared with other ArF processes)	
2 wafer transport systems @ 5,000	= 10,000
1 tri methylaluminum gas @ 100,000	= 100,000
transport and recovery/scrubber system	
Installation	= 8,000
Salvage value	= <u>(1,000)</u>
EQPT TOTAL	= \$ 203,000

2. **FT2** - Based on a preliminary estimate of 30 FT² for the scrubber system, total facility area = 138 FT².

3. **DLAB** - Maintenance for the two lasers is based on required thyatron replacement, with an additional two hr/week devoted to the reactant gas scrubber. Facility operation is assigned to one full time operator per shift:

Operation = 4160/yr @ \$6 = \$ 24,960
Maintenance = 740 hr/yr @ \$10 = \$ 7,400
DLAB TOTAL = \$ 32,360

4. **MATLS** - Replacement parts for the two lasers are based on thyatron replacement and weekly parts refurbishment

previously described. Excimer gas consumption with the gas scrubber was calculated at slightly less than \$0.05/hr. Preliminary calculations of reactant gas consumption, assuming that N₂ is used as the carrier, show insignificant usage. Calculated material costs are:

Gas consumption, annual (ArF)	= \$ 173
Thyratron replacement @ 6 week intervals:	= \$ 38,280
2 lasers x 8.7/yr @ \$2,200	
Weekly part refurbish @ cost of \$417/laser (2)	= \$ 5,136
Part replacement monthly @ cost of \$1250/laser	= \$ <u>30,000</u>
MATLS TOTAL	= \$ 73,589

5. UTIL - Annual KWHRS for equipment were estimated at:

Wafer transport	= 1,768 KWHR
Thyratrons	= 10,404 KWHR
Gas reprocessing	= 694
Scrubber	= <u>1,768</u>
UTIL TOTAL @ \$0.075/KWHR	= \$ 1,097

(d) Laser Oxide Passivation Initiation and Oxide Growth

1. EQPT - Two facility setups are required using identical lasers but operating at different rates due to process dwell time to control the oxide thickness. One setup deposits only 15 to 20Å and accomplishes the required deposition rates/wafer with only one ArF laser. Second stage, performed subsequent to the laser metallization process described above produces oxides grown to approximately 75Å and hence requires proportionally longer process times. Equipment types for the two facilities is identical varying only in that there are two lasers employed in the growth step. The gas processor, source gas scrubber and K-bottle bank costs are split on a 30:70 basis between the facilities:

For oxide passivation:

1 EXC-2 laser	= \$27,000
1 N/C table	= 10,000
1 Microprocessor	= 3,000
3/10 scrubber	= 30,000
3/10 gas reprocess	= 3,000
Cell transport	= 7,500
K-bottle farm	= <u>1,000</u>
PASSIVATION EQPT TOTAL	= \$81,500

For oxide growth equipment costs are:

2 EXC-2 ArF lasers	= \$ 54,000
7/10 gas processor	= 7,000
1 microprocessor	= 3,000
2 N/C tables	= 10,000

K-bottle bank = 1,000
 7/10 source gas scrubber = 70,000
 OXIDE GROWTH EQPT TOTAL = \$155,000

2. FT² - An additional 20 FT² of facilities area is required due to the second laser. The passivation process is allocated 78 FT² and the growth step. 98 FT².
3. DLAB - The passivation facility operates at only 1.3 shifts/day to achieve the 650 wafer/hour rate. Maintenance labor is assumed to be required at 67% of the normal rate for full shift operation. For this step, the direct labor is:

Operators = 1.3 shifts x 2080 Hr @ \$6 = \$ 16,224
 Maintenance = 175 Hr/Yr @ \$10 = 1,750
 PASSIVATION DLAB TOTAL = \$17,974

By contrast, to achieve 650 wafers per hour, the oxide growth facility has 1.5 operators assigned full time for two shifts. Maintenance labor is equal to that of the laser metallization process:

1 Operator/shift @ \$6 = \$ 24,960
 1/2 Sr. Processor/shift @ \$8 = 16,640
 Maintenance 740 Hr/Yr @ \$10 = 7,400
 OXIDE GROWTH DLAB TOTAL = \$48,000

4. MATLS - Direct materials costs for these two similar processes are assumed to be proportional to the laser front contact metallization at directly and by twofold respectively.
5. UTIL - The KWHR estimates for both processes were based on predicted rates for the laser metallization process adjusted for relative cost sharing.

6.0 PROGRAM STATUS AND PLANS

The project goal to produce 16.5% cells has not yet materialized. Major problems are believed to be beam nonuniformity and the deep channeling distance of $31p^+$ ions, even at 5 keV. Improvement to the beam uniformity is in progress by installation of a kaileoscope as described in Section 4.2. Low keV ion implantation would reduce the ion channeling distance which requires lower annealing energy, leaving the surface less damaged at the overlap area. However, at the time of this report, the lowest keV available is 5 keV.

An alternate approach is to use an n-type substrate with a boron ion implant which will have lower penetration depth and has been reported to produce 16.5% efficiency (R. Young, App. Phys. Lett. 1983) on 1×2 cm² cell area.

During the next quarter work will focus on developing the laser annealing process for boron ion implantation and developing a capability for uniform dopant incorporation.

Figure 27 shows the program status.

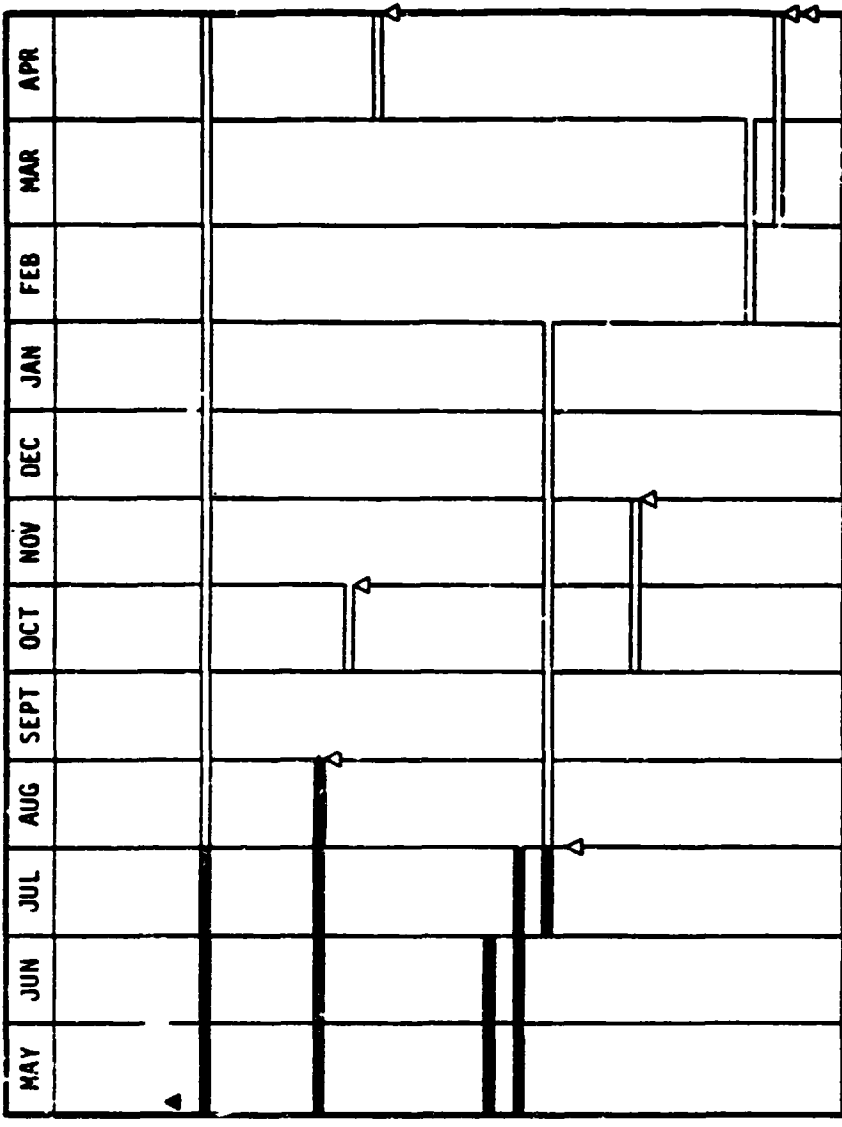


Fig. 27. Program Schedule.

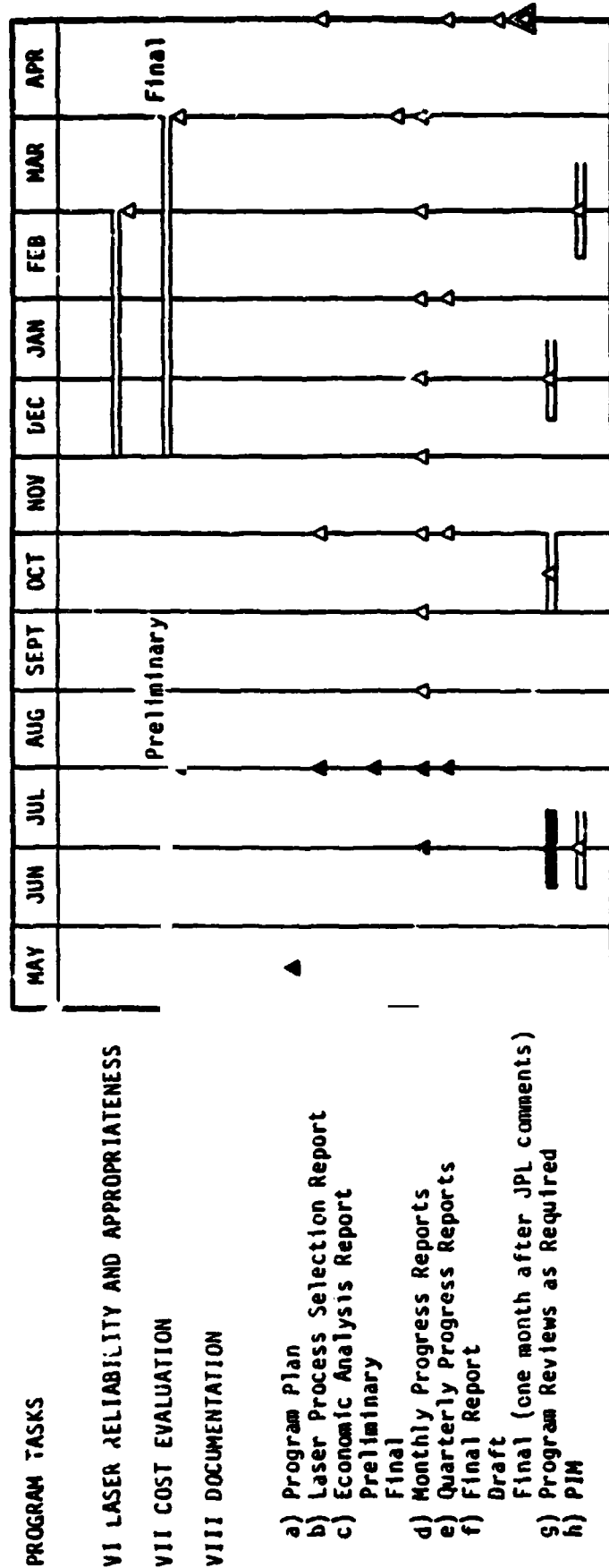


Fig. 27. Program Schedule (Continued).

REFERENCES

Hovel, Harold. Semiconductors and Materials, Vol. 2, p. 40, 1975

Young, R.T., Van der Leeden, G.A., Narayan, J., Christie, W.H., Wood, R.F., Rothe, D.G., and Levanther, J.I. IEEE Electron Device Letters, Vol. EDL-3, No. 10, 1982.

Lockheed Quarterly Report No. 2, JPL Contract 955696, 1980.

Young, R.T., Van der Leeden, G.A., Wood, R.F. and Westbrook, R.D. Applied Physics Letters, 43 (7), p. 666, 1983.

PRECEDING PAGE BLANK NOT FILMED